

# **Global Two-Channel AVHRR Retrievals of Aerosol Properties over the Ocean for the Period of NOAA-9 Observations and Preliminary Retrievals Using NOAA-7 and NOAA-11 Data**

IGOR V. GEOGDZHAYEV

*Columbia University/NASA GISS, New York, New York*

MICHAEL I. MISHCHENKO AND WILLIAM B. ROSSOW

*NASA Goddard Institute for Space Studies, New York, New York*

BRIAN CAIRNS

*Columbia University/NASA GISS, New York, New York*

ANDREW A. LACIS

*NASA Goddard Institute for Space Studies, New York, New York*

---

*Corresponding author address:* Dr. Michael Mishchenko, NASA Goddard Institute for Space Studies, 2880 Broadway, New York, NY 10025. E-mail: [crmim@giss.nasa.gov](mailto:crmim@giss.nasa.gov).

## ABSTRACT

We describe an improved algorithm which uses channel 1 and 2 radiances of the Advanced Very High Resolution Radiometer (AVHRR) to retrieve aerosol optical thickness and Ångström exponent over the ocean. We specifically discuss recent changes in the algorithm as well as the results of a sensitivity study analyzing the effect of several sources of retrieval errors not addressed previously. Uncertainties in the AVHRR radiance calibration (particularly in the deep-space count value) may be among the major factors potentially limiting the retrieval accuracy. A change by one digital count may lead to a 50% change in the aerosol optical thickness and a change of 0.4 in the Ångström exponent. On the other hand, the performance of two-channel algorithms weakly depends on a specific choice of the aerosol size distribution function with less than 10% changes in the optical thickness resulting from replacing a power law with a bimodal modified log normal distribution. The updated algorithm is applied to a 10-year period of observations (July 1983–Aug 1994), which includes data from NOAA-7, NOAA-9 (February 1985–November 1988), and NOAA-11 satellites. The results are posted on the world wide web at <http://gacp.giss.nasa.gov/retrievals>.

The NOAA-9 record reveals a seasonal cycle with maxima occurring around January-February and minima in June-July in the globally averaged aerosol optical thickness. The NOAA-7 data appear to show a residual effect of the El Chichon eruption (March 1982) as increased optical thickness values in the beginning of the record. The June 1991 eruption of Mt Pinatubo resulted in a sharp increase in the aerosol load to more than double its normal value. The NOAA-9 record shows no discernable long-term trends in the global and hemisphere averages of the optical thickness and Ångström exponent. On the other hand, there is a discontinuity in the Ångström exponent values derived from NOAA-9 and NOAA-11 data and a significant temporal trend in the NOAA-11 record. The latter are unlikely to be related to the Pinatubo eruption and may be indicative of a serious calibration problem.

The NOAA-9 record shows that the Northern hemisphere mean optical thickness systematically exceeds that averaged over the Southern hemisphere. Zonal means of the optical

thickness exhibit an increase in the tropical regions of the Northern hemisphere associated with annual desert dust outbursts and a spring time increase at middle latitudes of the Northern hemisphere. Increased aerosol loads observed at middle latitudes of the Southern hemisphere are probably associated with higher sea salt particle concentrations. Reliable extension of the retrieval record beyond the NOAA-9 lifetime will help to corroborate these findings.

## **1. Introduction**

Improved predictions of climate variability based on general circulation models require reliable knowledge of the global aerosol distribution in the Earth's atmosphere. The existing satellite datasets with their long-term record and near global coverage are a unique source of information about atmospheric aerosols. Accordingly, one of the objectives of the Global Aerosol Climatology Project (GACP, <http://gacp.giss.nasa.gov>) established in 1998 as part of NASA's Radiation Science Program and the Global Energy and Water Cycle Experiment is to perform a retroactive analysis of the NOAA AVHRR radiance dataset in order to infer the global distribution of aerosols, their properties, and seasonal and interannual variations. This paper describes research results obtained within the framework of the GACP and is a logical continuation of the recent paper by Mishchenko et al (1999a).

Because strong temporal and spatial variability of tropospheric aerosols may limit the accuracy of AVHRR aerosol retrievals using only channel 1 radiances (Ignatov et al. 1995; Stowe et al. 1997), it has been suggested that the use of channel 2 as well as channel 1 radiances may improve the accuracy of retrieving the aerosol optical thickness as well as provide an estimate of the aerosol particle size (Durkee et al. 1991; Nakajima and Higurashi 1998). Still with only two pieces of data per pixel available, one can retrieve only two model parameters and must assign fixed global values to the remaining parameters, thereby introducing potential significant biases in the aerosol product. In a recent paper (Mishchenko et al. 1999a), we used the actual AVHRR data to analyze the sensitivity of monthly averages of the aerosol optical thickness and size to various *a priori* assumptions incorporated in two-channel retrieval

algorithms as well as to adopting a specific cloud-screening procedure. We also reported preliminary retrieval results based on the post-launch International Satellite Cloud Climatology Project (ISCCP; Rossow and Schiffer 1999) calibration of channel 1 radiances and the pre-launch calibration of channel-2 radiances.

This paper first describes several recent improvements in the base retrieval procedure, including the use of the National Oceanic and Atmospheric Administration (NOAA) post-launch calibration of channel-2 radiances instead of the pre-launch calibration, and analyze the sensitivity of the aerosol product to additional factors and alternative cloud screening strategies not specifically addressed by Mishchenko et al. (1999a). We then use the updated version of the retrieval algorithm to derive a global climatology of aerosol properties over the ocean for the full period of NOAA-9 observations and briefly discuss its main features. Preliminary retrievals using NOAA-7 and NOAA-11 observations are also presented. We conclude by a discussion of our main results and future plans.

## **2. Revised retrieval algorithm**

Our retrievals are based on analyzing AVHRR channel 1 and 2 radiance data over the oceans provided by the gridded ISCCP DX dataset (Rossow et al. 1996). The availability of only two pieces of data per pixel makes inferring aerosol properties a highly underdetermined process in which one must fix all model parameters but two *a priori*. The traditional (and most rational) choice for the two retrieved parameters is the aerosol optical thickness and a measure of the aerosol particle size. As was shown by Mishchenko et al. (1999a), the latter should be the dimensionless Ångström exponent rather than a specific parameter of the aerosol size distribution such as the mode or effective radius.

In the current version of the retrieval algorithm, we assume that aerosol particles are homogeneous spheres and compute their scattering and absorption properties using the standard Lorenz-Mie theory (Mishchenko et al. 2002). The respective computer code was described by Mishchenko et al. (1999b) and is available at <http://www.giss.nasa.gov/~crmim>. Theoretical

channel 1 and 2 reflectances are then calculated using a radiative transfer code based on the scalar version of the adding/doubling method (Hansen and Travis 1974). The numerical procedure incorporates the rough ocean surface reflection via the modified Kirchhoff approximation (Mishchenko and Travis 1997), the water vapor, oxygen, and CO<sub>2</sub> absorption via the k-distribution technique (Lacis and Oinas 1991), and gaseous (Rayleigh) scattering. The upwelling radiances from the ocean body and foam scattering are either ignored or modeled by adding a small Lambertian component to the surface bidirectional reflection function. The atmospheric temperature and humidity profiles are taken from the ISCCP version of the Television and Infrared Observation Satellite (TIROS) Operational Vertical Sounder (TOVS) data, while the vertical distribution of ozone and water vapor is based on a standard atmospheric profile (McClatchey et al. 1972). The vertical profile of aerosol is taken to be the same as the normalized profile of water vapor. The radiative transfer code is used to compute a look-up table in which multidimensional arrays of theoretical channel 1 and 2 reflectance values for all viewing geometries and aerosol and atmospheric parameters are stored. The look-up table is then used to retrieve the aerosol optical thickness and size using cloud-screened channel 1 and 2 radiance data. Each pixel is mapped on a 1° by 1° global grid. The retrieved values of the aerosol parameters for all pixels within one grid cell are averaged to produce a map for a specified period of time. A more detailed description of the retrieval process was provided by Mishchenko et al. (1999a).

The updated version of the retrieval algorithm as well as the original version described by Mishchenko et al. (1999a) are based on the power law aerosol size distribution of the form

$$n(r) = \begin{cases} C, & r \leq r_1, \\ C \left( \frac{r}{r_1} \right)^{-\alpha}, & r_1 < r \leq r_2, \\ 0, & r > r_2 \end{cases} \quad (1)$$

with  $r_1 = 0.1 \mu\text{m}$ ,  $r_2 = 10 \mu\text{m}$ , and  $\alpha \in [2.5, 5]$ . The normalization constant  $C$  is chosen such that

$$\int_0^{\infty} dr n(r) = 1.$$

This analytical representation of the aerosol size distribution is very simple and yet appears to approximate well the actual size distributions in many cases (e.g., Russell et al. 1999; Francis et al. 1999; Hignett et al. 1999). The Ångström exponent  $A$  is defined as

$$A = \left. \frac{d[\ln C_{\text{ext}}(\lambda)]}{d(\ln \lambda)} \right|_{\lambda=\lambda_1}, \quad (2)$$

where  $\lambda_1 = 0.65 \mu\text{m}$  is the nominal wavelength of AVHRR channel 1 and  $C_{\text{ext}}$  is the ensemble-averaged extinction cross section per particle. The relationship between the Ångström exponent and the power exponent  $\alpha$  is illustrated by Fig. 3 of Mishchenko et al. (1999a).

Compared to the initial choice of the aerosol refractive index  $1.5 + 0.005i$  (Mishchenko et al. 1999a), the imaginary part has been reduced to 0.003, the reason being that this may help to achieve a better balance between the non-absorbing sea salt aerosols and the absorbing anthropogenic and dust aerosols on the global scale. The refractive index is assumed to be wavelength-independent. Figure 1 is a contour plot of the ratio of the phase functions for the two refractive indices versus scattering angle and Ångström exponent. Obviously, the two phase functions are close everywhere except at backscattering angles, where the differences can exceed 25%. The differences are greater for larger particles and decrease as the Ångström exponent increases. Figure 2 depicts the single-scattering albedo versus the Ångström exponent for the two refractive indices used in the updated and the original algorithm. Also shown is the ratio of the latter to the former. The greatest differences (about 7%) occur for the largest particles and decrease (down to 2%) with decreasing particle size. In the single-scattering approximation, the retrieved aerosol optical thickness is inversely proportional to the product of the single-scattering albedo and the phase function. Therefore, the decrease in the imaginary part of the refractive index in the revised algorithm causes an overall reduction in the retrieved optical thickness, the effect being stronger for larger particles. One should note, however, that while we feel that these

changes provide a better microphysical description of the aerosol observed most frequently over the oceans, it is impossible to develop a single optical model for aerosols as diverse in size and chemical composition as sulfate, sea salt, soot, and dust particles. Instead, we hope that a model can eventually be constructed that provides the best match to the mean global values of the optical thickness and size derived with more advanced satellite sensors such as the Multiangle Imaging Spectro-Radiometer (MISR) (Kahn et al. 1998, 2001), the MODerate resolution Imaging Spectrometer (MODIS) (King et al. 1992; Tanré et al. 1997), and the POLarization and Directionality of Earth Reflectances (POLDER) instrument (Goloub et al. 1999; Deuzé et al. 2000).

An additional change in the algorithm is related to the treatment of the ocean bidirectional reflectance. The initial algorithm included only the specular reflection from the rough ocean surface according to the modified Kirchhoff approximation (Tsang et al. 1985; Mishchenko and Travis 1997). The distribution of ocean surface slopes was assumed to be Gaussian:

$$P\left(\frac{\partial z}{\partial x}, \frac{\partial z}{\partial y}\right) = \frac{1}{2\pi s^2} \exp\left(-\frac{(\partial z/\partial x)^2 + (\partial z/\partial y)^2}{2s^2}\right), \quad (3)$$

where the mean square surface slope  $s^2$  is related to the near-surface wind speed  $W$  (m/s) via the empirical formula of Cox and Munk (1954):

$$2s^2 = 0.003 + 0.00512W. \quad (4)$$

However, according to the ocean color research (e.g., Spinrad et al. 1994 and references therein), there is also a small Lambertian component caused by multiple scattering of light by dissolved and particulate matter and chlorophyll pigments in the ocean body. It varies from almost zero for clean open ocean areas to 0.1 for polluted coastal zones. Since clean waters are likely to represent a larger fraction of the entire oceanic area over which aerosol retrievals are performed, we have adopted in the revised algorithm a spatially uniform wavelength-independent value of 0.002 for the diffuse reflection coefficient. This change may also help to reduce the effect of increasing the ocean reflectance by undetected whitecaps (Frouin et al. 1996; Moore et al. 1998).

Our computations have shown that the combined effect of increasing the model reflection

coefficient of the ocean and decreasing the imaginary part of the aerosol refractive index is a nearly uniform reduction in the retrieved optical thickness. The uniformity of this change is explained by the fact that the reduction in the aerosol absorption has the strongest effect in areas with high aerosol loads, whereas the effect of the increase in the ocean reflectance is most pronounced in the case of optically thin aerosols (Mishchenko et al. 1999a).

Previous studies have shown that the uncertainty in the retrieved Ångström exponent increases with decreasing aerosol optical thickness (Ignatov et al, 1998; Higurashi and Nakajima 1999). In addition, since smaller optical thicknesses correspond to smaller radiances for a given scattering geometry, the retrieval results become increasingly dependent on the calibration and digitization of AVHRR radiances and, in particular, on the value of the so-called “deep space” count (Rao et al. 1993), thereby rendering the retrieval results unreliable. Detailed analyses of the retrieval process have revealed that in many cases the range of uncertainty in the retrieved Ångström exponent can exceed the range of its expected natural variability. As a consequence, we have found that for some pixels the best retrieval in terms of yielding the minimal difference between the measured and modeled radiances is obtained for Ångström exponents corresponding to either the maximal or the minimal  $A$  value allowed by our look-up tables. The effect is clearly discernable in the maps of the monthly mean Ångström exponent (Fig. 3). A histogram of Ångström exponent values (Fig. 4) shows a rather uniform frequency of occurrence of different Ångström exponent values within the range  $[0, 1.75]$  allowed by our look-up tables with two relatively weak maxima at  $A \approx 0.3$  (attributable to outflows of larger dust particles from continents) and  $A \approx 1.1$ . This creates a problem of how the pixels yielding either  $A = 0$  or  $A = 1.75$  should be treated. For example, very small retrieved Ångström exponents correspond to large particles and may be interpreted as a sign of undetected cloud contamination. Alternatively, the cases of out-of-range Ångström exponent values may be caused by imperfect radiance calibration or result from using fixed global values of certain model parameters that are significantly different from their actual values for specific pixels at the time of the measurement.

In the original version of the algorithm, such pixels were allowed to contribute to the mean

$\tau$  and A values. However, given the above-mentioned uncertainty, we decided to modify the final aerosol product by creating two separate Ångström exponent datasets which may be called “constrained” and “unconstrained” versions. In the unconstrained version, all pixels are taken into account in computing the average A value, whereas the constrained version excludes pixels with  $A = 0$  or  $A = 1.75$ . In both cases all pixels contribute to the optical thickness average.

As mentioned by one of the reviewers of this paper, another way of dealing with this problem could be to restrict the retrieval of the Ångström exponent to cases where the optical thickness is greater than a minimum threshold value (see also Higurashi and Nakajima 1999). This suggestion is based on the assumption that the effect of calibration uncertainties and other negative factors should decrease with increasing optical thickness and the observation that Ångström exponent retrievals may become less reliable with decreasing aerosol load. It might be argued that in a certain sense, the approach employed in this paper implicitly uses a variable cutoff value of the optical thickness instead of a fixed one, and also removes the cases that cannot be adequately represented by the model used in the retrieval algorithm.

Another change in the revised algorithm is imposing certain limits on the allowed observational geometry. Specifically, all pixels with solar zenith angles exceeding  $70^\circ$  and/or satellite zenith angles exceeding  $60^\circ$  are rejected. The purpose of these limits is to eliminate extreme cases of grazing illumination and/or reflection which may not be adequately described by the radiative transfer model’s plane-parallel atmosphere assumption.

The final change is the use of the post-launch calibration of channel 2 radiances (Rao et al. 1993) instead of the pre-launch calibration in order to account for the degradation of the detector sensitivity. The consequences of this change will be discussed in Section 3.b.

### **3. Further sensitivity analyses**

Mishchenko et al. (1999a) performed a detailed sensitivity study of two-channel aerosol retrievals using the original version of the data analysis algorithm and the pre-launch channel 2 calibration. In this section, we will reassess their key findings by using the updated algorithm

and the post-launch calibration of channel 2 radiances and will supplement their analysis by considering additional sources of retrieval errors.

### *a. Cloud screening*

As discussed by Mishchenko et al. (1999a), cloud screening is a very important issue for aerosol retrievals from space. In our algorithm we use the ISCCP cloud detection scheme (Rossow and Garder 1993), which is based on a successive application of space- and time-contrast tests and temperature and radiance thresholds. In addition, we require that only pixels with infrared temperature warmer than the composite temperature by 1 K or more be retained, which makes the cloud screening algorithm more conservative and provides better identification of pixels potentially contaminated by thin cirrus or subpixel patches of cumulus clouds.

Durkee et al. (2000) proposed a dynamic reflectance threshold test for AVHRR aerosol retrievals over the 2nd Aerosol Characterization Experiment (ACE-2) region (Raes et al. 2000; Russell and Heintzenberg 2000). According to that test, a pixel is removed if the corresponding channel 2 reflectance is greater than 15% and the channel 4 temperature is greater than the channel 5 temperature. We have found that the global effect of applying this test is marginal, and that in many cases it is unable to remove high  $\tau$  values in polar regions.

Stowe et al. (1999) used a near-infrared channel 3 albedo test as part of their cloud screening algorithm to detect weakly reflecting clouds. Since this channel is contaminated by thermal emission, it must be corrected for by using radiative temperatures from infrared channels 4 and 5. Stowe et al. suggested rejecting the pixels with the corrected channel 3 albedo greater than 3% over the ocean. We have implemented this test in order to study its effect on our retrievals and found that depending on the threshold channel 3 albedo value, the superimposition of the test on our cloud screening procedure (ISCCP cloud tests plus IR thresholds) either has negligible effect or removes pixels in the areas with high aerosol loads such as regions of Saharan dust outflows. Note that Stowe et al. also indicated that the test affected only trace amounts of ocean pixels that passed the rest of the cloud screening tests.

In the original version of the retrieval algorithm, we also used a channel 1 to channel 2 radiance ratio  $S_{12}$  criterion (Wagener et al. 1997). We have found that the application of this criterion on top of the cloud screening procedure based on the AVHRR infrared channels has only marginal effect, mostly removing spurious cases of large optical thickness at higher latitudes. We have since discovered that this criterion has an undesirable property of being sensitive to the relative calibration of the two visible AVHRR channels. In addition, it sometimes rejects pixels with high aerosol loads that do not exhibit sufficient spectral contrast in areas such as the Atlantic ocean off the west coast of Africa and Persian Gulf. These areas are dominated by outflows of large dust particles, as indicated by small retrieved values of the Ångström exponent. Therefore, we have replaced the  $S_{12}$  criterion with a somewhat simplistic requirement that pixels with retrieved optical thickness higher than 0.6 be rejected if they occur north of 50°N or south of 50°S. This requirement has only a minor effect on the retrievals and serves mainly the purpose of removing the spurious cases of anomalously high  $\tau$  at high latitudes presumably caused by ice, foam, or cloud contamination of the pixel.

### *b. Radiance calibration*

Since AVHRR does not have an in-flight calibration capability, a number of vicarious calibration techniques have been proposed in order to account for the temporal degradation of the instrument (e.g., Che and Price 1992; Kaufman and Holben 1993, Rao and Chen 1995). This is accomplished by determining the coefficients of a linear regression expressing the absolute radiance in terms of the instrument digital counts:

$$I = \alpha(CT - CT_0), \quad (5)$$

where  $I$  [ $\text{W m}^{-2} \mu\text{m}^{-1} \text{sr}^{-1}$ ] is the absolute radiance,  $\alpha$  [ $\text{W m}^{-2} \mu\text{m}^{-1} \text{sr}^{-1}$ ] the gain, CT the ten-bit digital count, and  $CT_0$  the offset (deep-space count). Most of the research has been focused on establishing the absolute value and time dependence of the gain assuming the pre-launch value of the deep space count, the paper by Brest and Rossow (1992) being a rare

exception. This is justified in the case of cloud and land surface remote sensing, because these objects are bright, and the difference  $CT - CT_0$  is large. However, for aerosol retrievals over the dark ocean surface, it is important to know  $CT_0$  with the maximum precision since the difference  $CT - CT_0$  is small.

Rao et al. (1993) pointed out that for the AVHRR instrument onboard NOAA-9, there is a 1–2 count spread in the published offset values, while the difference between the pre-launch and the post-launch values could be as large as 3.5 counts. Given this uncertainty, it is important to analyze the sensitivity of the retrieved aerosol optical depth and Ångström exponent to potential changes in the offset value. As we have already mentioned, the revised algorithm uses the ISCCP post-launch calibration of channel 1 radiances (Brest et al. 1997) and the NOAA post-launch calibration of channel 2 radiances (Rao et al. 1993). Figure 5 shows the ratio of monthly mean aerosol optical thicknesses [panel (a)] and the difference of Ångström exponents [panel (b)] retrieved with modified (reduced by one count) and original channel 2 radiances. The obvious result is a decrease in the aerosol optical thickness of up to 50% and an increase in the Ångström exponent of up to 0.4. Both effects are caused by the implicit increase in the spectral contrast of the aerosol contribution to the total radiance. The addition of one digital count to channel 2 radiances [Figs. 5(c) and 5(d)] can cause a 50% increase in the optical thickness and a 0.4 decrease in the Ångström exponent. Not surprisingly, the biggest errors occur in areas with small aerosol loads (cf. Higurashi and Nakajima 1999).

One of the reviewers of this paper has suggested that calibration errors may in fact be significantly smaller than  $\pm 1$  count, at least when data from a single satellite (e.g. NOAA-14) are considered. If this is indeed the case, the retrieval errors caused by calibration uncertainties can also be significantly smaller.

### *C. Sensitivity to choice of aerosol size distribution function*

In order to study the effect of using a specific analytical representation of the aerosol size

distribution, we have performed retrievals using a modified log normal distribution of the form (Nakajima and Higurashi 1998)

$$n(r) = C_1 r^{-4} \left[ \exp\left(-\frac{(\ln r - \ln r_{g1})^2}{2 \ln^2 \sigma_{g1}}\right) + \gamma \exp\left(-\frac{(\ln r - \ln r_{g2})^2}{2 \ln^2 \sigma_{g2}}\right) \right] \quad (6)$$

with  $r_{g1} = 0.17 \mu\text{m}$ ,  $r_{g2} = 3.44 \mu\text{m}$ ,  $\sigma_{g1} = 1.96$ ,  $\sigma_{g2} = 2.37$ , and  $\gamma \in [0.1, 100]$ . Figure 6 shows the ratio of monthly mean optical thicknesses [panel (a)] and the difference of constrained monthly mean Ångström exponents [panel (b)] retrieved using the bimodal log normal and the power law size distributions for July of 1986. The differences in  $\tau$  rarely exceed 10%, while the differences in  $A$  range between  $-0.1$  and  $0.35$ . The differences between unconstrained monthly mean Ångström exponents (not shown) are similar.

These results corroborate those reported by Mishchenko et al. (1999a) [compare panels (a) and (b) of Fig. 6 and their Figs. 15(a) and 15(b)]. Note that although they used different assumptions about the aerosol refractive index and the ocean reflectance as well as the pre-launch channel 2 calibration, the range of the potential uncertainty associated with choosing different size distribution functions was essentially the same. The small optical thickness differences can undoubtedly be explained by the higher flexibility of two channel retrieval procedures compared to single-channel algorithms using a fixed aerosol phase function.

#### *d. CCN column number density*

Because of the complexity of physical and chemical processes involved, the indirect aerosol radiative forcing is one of the largest unknown factors in climate research (Hansen et al. 1998; Brenguier et al. 2000; Haywood and Boucher 2000). An important variable needed for modeling these processes is the number density of cloud condensation nuclei (CCN) (Schwartz and Slingo 1996). If the aerosol optical thickness  $\tau$  is known, it follows directly from the definitions of  $\tau$  and  $C_{\text{ext}}$  that the CCN column number density  $N_{\text{CCN}}$  can be calculated as

$$N_{\text{CCN}} = \frac{\tau}{C_{\text{ext}}}, \quad (7)$$

where  $C_{\text{ext}}$  is the ensemble-averaged extinction cross section per particle. Using a two-channel retrieval algorithm, we can determine  $C_{\text{ext}}$  for each pixel from the retrieved Ångström exponent and the assumed analytical representation of the size distribution (cf. Fig. 3 of Mishchenko et al. 1999a) and then determine  $N_{\text{CCN}}$  from Eq. (7). Figure 7 shows the extinction cross section versus the Ångström exponent for the bimodal log normal and power law size distributions. Also shown is their ratio. It is seen that for a given value of the Ångström exponent, the extinction cross section is always greater for the power law distribution. The extinction cross section ratio can be as small as 0.2 for large particles (small Ångström exponents) and approaches unity as the Ångström exponent increases. Differences in  $C_{\text{ext}}$  as large as a factor of five suggest that CCN column number density retrievals based on two-channel algorithms are strongly dependent on the choice of the size distribution type. This is illustrated by Figs. 6(c) and 6(d), which depict the ratio of monthly mean CCN column densities calculated using the bimodal log normal and the power law size distribution. Figure 6(c) illustrates the constrained Ångström exponent retrieval and shows differences as large as a factor of 3. The use of unconstrained A values [Fig. 6(d)] reduces the differences because the overall increase of A causes the extinction cross section ratio to be closer to unity (Fig. 7). Yet the  $N_{\text{CCN}}$  differences can still exceed a factor of 2.5.

One may thus conclude that the error margin of CCN column number densities retrieved from two-channel AVHRR data can be unacceptably high for climate research applications. This result corroborates the theoretical findings of Mishchenko et al. (1997a), who performed a sensitivity study of various passive remote sensing techniques for retrieval of aerosol column densities over the ocean. Based on radiative transfer calculations they demonstrated poor performance of single-viewing-angle, radiance-only AVHRR-type algorithms in CCN column number density retrievals. The authors explain this by the strong dependence of the extinction

cross section and weak dependence of the phase function on the aerosol effective radius. The research suggested that high-precision multiangle and multispectral polarization measurements (Cairns et al. 1999; Mukai and Sano 1999; Deuzé et al. 2000; Masuda et al. 2000; Kawata et al. 2000; Chowdhary et al. 2001) should provide significantly more accurate retrievals.

#### *e. Effect of wind speed*

Mishchenko et al. (1999a) studied the sensitivity of AVHRR aerosol retrievals to the near-surface wind speed by comparing retrievals performed assuming two fixed wind speed values. To extend their analysis, we have employed the assimilation database derived by Atlas et al. (1996) from the Special Sensor Microwave Imager (SSM/I) observations, model analyses, and ship and buoy reports. Specifically we have used level 3.0 uniform space-time gridded wind speed values specified on a 2° latitude, 2.5° longitude, 6 hour grid. A set of look-up tables corresponding to wind speed values of 5, 7, and 11 m/s was used. The wind speed value in the closest space-time grid cell was used to decide which lookup table must be used in aerosol retrievals for each pixel. Pixels with wind speed values exceeding 12 m/s were rejected as potentially contaminated by a significant reflectance contribution from whitecaps.

Figure 8 illustrates the effect of wind speed on two-channel aerosol retrievals. Figure 8(a) shows the ratio of monthly mean aerosol optical thicknesses for July 1987 retrieved using the SSM/I database and assuming a fixed global value of 7m/s. Figure 8(b) shows the difference of respective constrained Ångström exponents. One can see that the retrieval errors due to the assumption of a fixed wind speed value do not exceed 10% in most cases. This is in agreement with the previous result of Mishchenko et al. (1999a). In addition, one can notice that the largest differences occur in regions with small aerosol loads [cf. Fig. 3(a)], where the relative contribution of the surface reflectance to the total measured radiance is the largest. Contrasting Fig. 8(a) with the respective map of the average wind speed for July 1987 (see <http://www.ssmi.com>) shows that the regions of the greatest overestimation of the aerosol optical thickness occur in areas with prevailing wind speeds higher than the assumed 7 m/s value.

According to Fig. 8(b), retrieval errors in the Ångström exponent caused by assuming a constant wind speed value are mostly within  $\pm 0.125$ . In regions with small aerosol loads and high wind speeds, the Ångström exponent can be underestimated by as much as 0.2. This can be explained by the fact that underestimating the contribution of the surface radiation by assuming a smaller wind speed value causes an effective reduction of the spectral contrast of the aerosol contribution to the total radiance in the two channels. One should remember however that these errors are still less than those associated with the choice of an aerosol size distribution function.

For a given region, there are seasonal patterns of the wind speed. Thus we may expect that the inclusion of the realistic wind speed data into the aerosol retrieval algorithm can improve the accuracy of aerosol retrievals on the regional scale, especially in areas with small aerosol loads. On the global scale, however, the small errors associated with choosing a fixed wind speed value are likely to be masked by other uncertainties.

#### **4. Global aerosol climatology**

The new algorithm has been applied to the ISCCP DX dataset (Rossow and Schiffer 1999) corresponding to the period of NOAA-9 observations (February 1995–November 1988). We have also added retrievals based on data from NOAA-7 and NOAA-11 so that the entire record covers more than 10 years from July 1983–August 1994. However, we consider the part of the record corresponding to the period of NOAA-7 and 11 observations preliminary for reasons discussed below. The resulting product is posted on the world wide web at <http://gacp.giss.nasa.gov/retrievals>.

Figures 9 and 10 show time series of the global and hemispherical means of the aerosol optical thickness and constrained (Fig. 9) and unconstrained (Fig. 10) Ångström exponents. The average aerosol load is systematically higher in the Northern hemisphere. It is easy to discern an annual variability pattern in the globally averaged aerosol optical thickness with maxima occurring around January-February and minima in June-July. The Northern hemisphere mean optical thickness follows a similar pattern, but with maxima in February–April. Similar findings

were reported by Stowe et al. (1997) and Husar et al (1997) based on analyses of July 1989–June 1991 data record using a one-channel retrieval algorithm. One can see the residual effects of the El Chichon (March 1982) eruption is visible as increased optical thickness values in the very beginning of the record. The June 1991 eruption of Mt Pinatubo resulted in a sharp increase in the aerosol load to more than double its normal value. The unconstrained average Ångström exponent is significantly greater than the constrained one. This may be explained by small residual errors in the AVHRR channel 1 and 2 calibration and the high sensitivity of Ångström exponent retrievals to such errors. The temporal behavior of both Ångström exponents exhibits less regularity than that of the optical thickness. The poor Ångström exponent retrieval accuracy makes further data record analyses less conclusive.

There is no discernable long-term trend in the global and hemisphere averages of the optical thickness and Ångström exponent during the NOAA-9 lifetime. Since our previous retrievals based on the pre-launch calibration of channel 2 radiances showed a significant increase of the Ångström exponent over the same period (Fig. 8 of Mishchenko et al. 1999a), this provides a strong indication that the ISCCP post-launch calibration of channel 1 and the NOAA post-launch calibration of channel 2 radiances do a good job in terms of correcting for the temporal degradation of the AVHRR detector sensitivity. Furthermore, since the drift of the NOAA-9 orbit caused a significant change in the time of observation at a particular point (and thus in the illumination geometry) over the lifetime of the satellite, the absence of a pronounced long-term trend may also indicate that the accuracy of the surface bidirectional reflectance modeling was sufficiently good and the two-channel algorithm was flexible enough (in terms of selecting an appropriate phase function for each pixel) as to introduce no systematic bias in the aerosol retrievals. Compared to the retrievals obtained using the initial version of the algorithm (cf. Fig. 8 of Mishchenko et al. 1999a), there is an overall reduction of the average global optical thickness value from about 0.19 down to about 0.15.

NOAA-11 data, on the other hand, exhibit a significant downward trend in the Ångström exponent that does not correlate with the fact that the Mt. Pinatubo eruption occurred in the

middle of the satellite lifetime. Furthermore the trend is opposite to what one would expect assuming that bigger particles had vanished faster after the eruption, thereby leading to an overall reduction in the particle size. Thus this trend as well as the obvious discontinuity in the Ångström exponent at the time of NOAA-9 to NOAA-11 transition may indicate a calibration problem, probably with the second AVHRR channel. Because of that, we consider the retrieval results for the periods of NOAA-7 and 11 observations preliminary and base the further analysis on the NOAA-9 record only.

## **5. Zonal mean values**

Zonal mean values of the aerosol optical thickness are of much interest since they are traditionally used in comparisons with and assessments of the accuracy of global circulation models and for other applications. Figure 11 is a contour plot of monthly zonal means of the aerosol optical thickness derived from the entire NOAA-9 dataset by mapping the data onto a  $5^\circ$  latitudinal grid for each month. Due to the specific character of the sun-synchronous orbit of the NOAA satellites, aerosol retrievals are possible within a latitudinal belt which varies from month to month. The exact boundaries of this belt change over time as the satellite orbit drifts. To avoid statistically insignificant cases at the boundaries of this belt, only cells with more than 20 individual data points were included. One can see that the aerosol load is systematically lower in the Southern than in the Northern hemisphere, in agreement with Fig. 9. The seasonal variability is also less pronounced in the Southern hemisphere due to the dominance of open ocean areas. A notable exception is the optical thickness increase at around  $40^\circ\text{S}$ , which may be associated with increased sea salt concentrations (cf. Higurashi et al. 2000 and Penner et al. 2001). In the Northern hemisphere, the significant seasonal variability in the tropics is explained by summer outflows of the Sahara dust and dust events in the Indian Ocean. Another interesting feature is an increase of the aerosol concentration at middle latitudes during the spring.

One should be cautioned that aerosol loads are highly variable from year to year depending on weather patterns and volcanic events. This makes it difficult to reliably identify long-term

regional and seasonal features. We hope, therefore, that extending the aerosol record beyond the NOAA-9 lifetime will allow us to characterize the seasonal and regional aerosol variability with larger certainty.

## 6. Conclusions, discussion, and future work

In this paper, we have described an improved version of the algorithm for retrieving aerosol properties from AVHRR channel 1 and 2 radiances. The algorithm has been used to build a (preliminary) global climatology of the aerosol optical thickness and Ångström exponent for a more than 10-year period that includes NOAA-7, 9, and 11 observations. The main results of the paper can be summarized as follows.

- Radiance calibration uncertainties may be among the main factors hampering the retrieval accuracy. Specifically, the addition/subtraction of one digital count to/from the AVHRR radiances can cause changes in the retrieved aerosol optical thickness exceeding 40% in open ocean areas. Given the significant spread in the published calibration constants, it is unlikely that a significant breakthrough in the retrieval accuracy may be achieved based on the AVHRR data alone. Instead, the way to solve the calibration problem may be to use advanced global satellite retrievals (Kahn et al. 1998, 2000; Tanré et al. 1997; Deuzé et al. 2000) as a benchmark.
- The two-channel algorithm shows a significant degree of insensitivity to a specific choice of the aerosol particle size distribution function. One should expect only small (.10%) changes in the retrieved aerosol optical thickness and changes less than 0.3 in the Ångström exponent when switching from one size distribution function to another. This conclusion appears to be independent of other model and calibration assumptions.
- The CCN column number density cannot be reliably retrieved from the two-channel AVHRR data. A change in the assumed analytical representation of the aerosol particle size distribution can lead to changes in the retrieved CCN concentration exceeding 300%.
- The assumption of a fixed global value of the wind speed leads to errors less than 10% in the

retrieved aerosol optical thickness and less than 0.125 in the Ångström exponent relative to the results obtained using real-time wind speed data. Taking real-time wind speed data into account may improve the accuracy of regional retrievals in the areas where strong wind patterns exist, although on the global scale the accuracy gain may be masked by other uncertainties.

- Global monthly mean values of the aerosol optical thickness show no significant trend over the lifetime of the NOAA-9 satellite (February 1985 through November 1988). The derived average global values are 0.15 for the optical thickness and 0.85 for the constrained Ångström exponent. However, these values depend on the assumed calibration and aerosol optical model, the main source of errors being the uncertainty in the deep space count.
- There is a discontinuity in the retrieved Ångström exponents at the time of NOAA-9 to NOAA-11 transition and a significant trend in the Ångström exponent not consistent with the Mt. Pinatubo eruption. This is likely to be an indication of a serious calibration problem.

This research will be continued and followed by processing data from other AVHRR instruments. This will require the development of a procedure to “reconcile” the calibration differences between different AVHRR instruments. The second direction of research will be the validation of the retrieval results (cf. Zhao et al. 2001). Since a two-channel algorithm can retrieve only two aerosol parameters and must rely on globally fixed values of all other model parameters, and because the retrieval accuracy can be plagued by factors such as imperfect cloud screening and calibration uncertainties, it appears more appropriate to talk about the “calibration” of the algorithm in terms of minimizing the difference between the actual and the retrieved global annual averages of the aerosol optical thickness and Ångström exponent. This effort will involve comparisons and consistency checks with other satellite, airborne, and ground-based datasets (e.g., Krotkov et al. 1999; Cakmur et al. 2001; Kinne et al. 2001) and models (e.g., Penner et al. 2001). This is not a simple task because of the scale differences, collocation problems, and different approaches to cloud screening. For example, good agreement with a limited ground-based or in situ dataset does not guarantee the global

applicability of the satellite-retrieved product. Ship aerosol data are scarce. The ground-based networks such as the Aerosol Robotic Network (AERONET) (Holben et al. 2000; Dubovik et al. 2000) and the Multi-Filter Rotating Shadowband Radiometer (MFRSR) network (Alexandrov et al. 2001) provide extensive coverage over land, but have only a few coastal sites, where the atmospheric conditions and surface albedo may be significantly different from those in the open ocean. An even greater challenge may be the improvement of the retrieval algorithm by adopting regional aerosol models which take into account, e.g., the stronger absorptivity of soot and dust-like particles (e.g., Fuller et al. 1999) and the nonsphericity of mineral aerosols (Liou and Takano 1994; Mishchenko et al. 1995, 1997b; Yang et al. 2000).

Kinne et al. (2001) and Penner et al. (2001) performed a comparison of monthly statistics of aerosol satellite retrievals and model results with the AERONET-derived statistics. Kinne et al. found that the aerosol optical thickness derived using the original algorithm described by Mishchenko et al. (1999a) are systematically higher compared to the averages from several coastal AERONET sites. Penner et al. used an intermediate GACP satellite product close to the one described in this paper and found a significantly better agreement. Both Kinne et al. and Penner et al. attributed the remaining discrepancies to differences in cloud screening techniques and aerosol optical model choices. Higher surface albedos in the coastal regions compared to the open ocean values assumed in the satellite retrievals may also have contributed to the discrepancies. Furthermore, the aerosol products were derived from NOAA-9 observations in the 1980s, whereas the AERONET data were collected in the 1990s.

Haywood et al. (2001) compared the aerosol optical thickness in the Saharan dust plume retrieved using a pyranometer onboard an airplane and two-channel AVHRR retrievals using the algorithm described here. They found that the AVHRR-derived optical thickness was generally within the  $\pm 0.1$  estimated error of the pyranometer-derived optical thickness provided that the time elapsed between the aircraft measurements and the AVHRR overpass was less than 3.75 hours. As the time between the two measurements increased, the magnitude of the differences increased too, but generally remained less than 30%. These results may illustrate the difficulties

in making comparisons between satellite and ground-based measurements when the two are separated by more than a few hours and/or are not spatially collocated to within a few tens of kilometers. It thus appears that an ideal way of fixing most if not all problems associated with the calibration of two-channel retrievals may be to use as a benchmark global long-term results of aerosol retrievals from more advanced instruments such as MISR, MODIS, and POLDER. Another useful technique for evaluating algorithm performance is self-consistency checks, where statistics are computed for large ensembles of the retrieval parameters as functions of other observed independent variables such as viewing geometry, latitude, etc. (e.g., Igantov and Stowe 2000, 2001). Obviously, all feasible approaches to validation should be pursued to gain the maximum understanding of the quality and uncertainties in the AVHRR retrievals.

*Acknowledgments.* We thank two anonymous reviewers for useful comments and suggestions and Nadia Zakharova for help with graphics. This research was sponsored by the NASA Radiation Science Program managed by Donald Anderson.

## References

- Alexandrov, M., A. Lacis, B. Carlson, and B. Cairns, 2001: MFRSR-based climatologies of atmospheric aerosols, trace gases and water vapor. *Proc. SPIE*, **4168**, 256–264.
- Atlas, R., R. Hoffman, S. Bloom, J. Jusem, and J. Ardizzone, 1996: A multiyear global surface wind velocity dataset using SSM/I wind observations. *Bull. Amer. Meteorol. Soc.*, **77**, 869–882.
- Brenguier, J. L., P. Y. Chuang, Y. Fouquart, D. W. Johnson, F. Parol, H. Pawlowska, J. Pelon, L. Schüller, F. Schröder, and J. Snider, 2000: An overview of the ACE-2 CLOUDY COLUMN closure experiment. *Tellus B*, **52**, 815–827.
- Brest, C. L., and W. B. Rossow, 1992: Radiometric calibration and monitoring of NOAA AVHRR data for ISCCP. *Int. J. Remote Sens.*, **13**, 235–273.
- Brest, C. L., W. B. Rossow, and M. D. Roiter, 1997: Update of radiance calibrations for ISCCP. *J. Atmos. Oceanic Technol.*, **14**, 1091–1109.
- Cairns, B., L. D. Travis, and E. E. Russell, 1999: The Research Scanning Polarimeter: Calibration and ground-based measurements. *Proc. SPIE*, **3754**, 186–197.
- Cakmur, R. V., R. L. Miller, and I. Tegen, 2001: A comparison of seasonal and interannual variability of soil dust aerosols over the Atlantic Ocean as inferred by the TOMS AI and AVHRR AOT retrievals. *J. Geophys. Res.*, in press.
- Che, N., and J. C. Price, 1992: Survey of radiometric calibration results and methods for visible and near infrared channels of NOAA-7, -9, and -11 AVHRRs. *Remote Sens. Environ.*, **41**, 19–27.
- Chowdhary, J., B. Cairns, M. Mishchenko, and L. Travis, 2001: Retrieval of aerosol properties over the ocean using multispectral and multiangle photopolarimetric measurements from the Research Scanning Polarimeter. *Geophys. Res. Lett.*, **28**, 243–246.
- Cox, C., and W. Munk, 1954: Statistics of the sea surface derived from Sun glitter. *J. Marine Res.*, **13**, 198–227.
- Deuzé, J. L., P. Goloub, M. Herman, A. Marchand, G. Perry, S. Susana, and D. Tanré, 2000:

- Estimate of the aerosol properties over the ocean with POLDER. *J. Geophys. Res.*, **105**, 15,329–15,346.
- Dubovik, O., A. Smirnov, B. N. Holben, M. D. King, Y. J. Kaufman, T. F. Eck, and I. Slutsker, 2000. Accuracy assessment of aerosol optical properties retrieved from Aerosol Robotic Network (AERONET) Sun and sky radiance measurements. *J. Geophys. Res.*, **105**, 9791–9806.
- Durkee, P., F. Pfeil, E. Frost, and E. Shima, 1991: Global analysis of aerosol particle characteristics. *Atmos. Environ. A*, **25**, 2457–2471.
- Durkee, P. A., K. E. Nielsen, P. J. Smith, P. B. Russell, B. Schmid, J. M. Livingston, B. N. Holben, C. Tomasi, V. Vitale, D. Collins, R. C. Flagan, J. H. Seinfeld, K. J. Noone, E. Öström, S. Gassó, D. Hegg, L. M. Russel, T. S. Bates, and P. K. Quinn, 2000: Regional aerosol optical depth characterisation from satellite observations: ACE-1, TARFOX and ACE-2 results. *Tellus B*, **52**, 484–497.
- Francis, P. N., P. Hignett, and J. P. Taylor, 1999: Aircraft observations and modeling of sky radiance distributions from aerosol during TARFOX. *J. Geophys. Res.*, **104**, 2309–2319.
- Frouin, R., M. Schwindling, and P.-Y. Deschamps, 1996: Spectral reflectance of sea foam in the visible and near-infrared: In situ measurements and remote sensing implications. *J. Geophys. Res.*, **101**, 14,361–14,371.
- Fuller, K. A., W. C. Malm, and S. M. Kreidenweis, 1999: Effects of mixing on extinction by carbonaceous particles. *J. Geophys. Res.*, **104**, 15,941–15,954.
- Goloub, P., D. Tanré, J. L. Deuzé, M. Herman, A. Marchand, and F.-M. Bréon, 1999: Validation of the first algorithm applied for deriving the aerosol properties over the ocean using the POLDER/ADEOS measurements. *IEEE Trans. Geosci. Remote Sens.*, **37**, 1586–1596.
- Hansen, J., M. Sato, A. Lacis, R. Ruedy, I. Tegen, and E. Matthews, 1998: Perspective: Climate forcings in the industrial era. *Proc. Natl. Acad. Sci.*, **95**, 12,753–12,758.
- Hansen, J. E., and L. D. Travis, 1974: Light scattering in planetary atmospheres, *Space Sci. Rev.* **16**, 527–610.

- Haywood, J. M., and O. Boucher, 2000: Estimates of the direct and indirect radiative forcing due to tropospheric aerosols: A review. *Rev. Geophys.*, **38**, 513–543.
- Haywood, J. M., P. N. Francis, I. V. Geogdzhayev, M. I. Mishchenko, and R. Frey, 2001: Comparison of Saharan dust aerosol optical depth derived using aircraft mounted pyranometers and 2-channel AVHRR retrieval algorithms. *Geophys. Res. Lett.*, **28**, 2393–2396.
- Hignett, P., J. P. Taylor, P. N. Francis, and M. D. Glew, 1999: Comparison of observed and modeled direct aerosol forcing during TARFOX. *J. Geophys. Res.*, **104**, 2279–2287.
- Higurashi, A., and T. Nakajima, 1999: Development of a two channel aerosol retrieval algorithm on global scale using NOAA/AVHRR. *J. Atmos. Sci.*, **56**, 924–941.
- Higurashi, A., T. Nakajima, B. N. Holben, A. Smirnov, R. Frouin, and B. Chatenet, 2000: A study of global aerosol optical climatology with two-channel AVHRR remote sensing. *J. Clim.*, **13**, 2011–2027.
- Holben, B. N., D. Tanré, A. Smirnov, T. F. Eck, I. Slutsker, N. Abuhassan, W. W. Newcomb, J. S. Schafer, B. Chatenet, F. Lavenue, Y. J. Kaufman, J. Vande Castle, A. Setzer, B. Markham, D. Clark, R. Frouin, R. Halthore, A. Karnieli, N. T. O’Neill, C. Pietras, R. T. Pinker, K. Voss, and G. Zibordi, 2000: An emerging ground-based aerosol climatology: Aerosol optical depth from AERONET. *J. Geophys. Res.*, **106**, 12,067–12,098.
- Husar, R. B., J. M. Prospero, and L. L. Stowe, 1997: Characterization of tropospheric aerosols over the oceans with the NOAA Advanced Very High Resolution Radiometer optical thickness operational product. *J. Geophys. Res.* **102**, 16889–16909.
- Ignatov, A., and L. L. Stowe, 2000: Physical basis, premises, and self-consistency checks of aerosol retrievals from TRMM/VIRS. *J. Appl. Meteorol.*, **39**, 2259–2277.
- Ignatov, A., and L. L. Stowe, 2001: Aerosol retrievals from individual AVHRR channels. II. Quality control, probability distribution functions, Information content, and consistency checks of retrievals. *J. Atmos. Sci.*, this issue.
- Ignatov, A. M., L. L. Stowe, S. M. Sakerin, and G. K. Korotaev, 1995: Validation of the

- NOAA/NESDIS satellite aerosol product over the North Atlantic in 1989. *J. Geophys. Res.*, **100**, 5123–5132.
- Ignatov, A., L. Stowe, and R. Singh, 1998: Sensitivity study of the Ångström exponent derived from AVHRR over the oceans. *Adv. Space Res.*, **21**, 439–442.
- Kahn, R., P. Banerjee, D. McDonald, and D. J. Diner, 1998: Sensitivity of multiangle imaging to aerosol optical depth and to pure-particle size distribution and composition over ocean. *J. Geophys. Res.*, **103**, 32,195–32,213.
- Kahn, R., P. Banerjee, D. McDonald, and J. Martonchik, 2001: Aerosol properties derived from aircraft multi-angle imaging over Monterey Bay. *J. Geophys. Res.*, in press.
- Kaufman, Y. J., and B. N. Holben, 1993: Calibration of the AVHRR visible and near-IR bands by atmospheric scattering, ocean glint and desert reflection. *Int. J. Remote Sens.*, **14**, 21–52.
- Kawata, Y., T. Izumiya, and A. Yamazaki, 2000: The estimation of aerosol optical parameters from ADEOS/POLDER data. *Appl. Math. Comput.*, **116**, 197–215.
- King, M. D., Y. J. Kaufman, W. P. Menzel, and D. Tanré, 1992: Remote sensing of cloud, aerosol, and water vapor properties from the Moderate Resolution Imaging Spectrometer (MODIS). *IEEE Trans. Geosci. Remote Sens.*, **30**, 2–27.
- Kinne, S., B. Holben, T. Eck, A. Smirnov, O. Dubovik, I. Slusker, D. Tanré, G. Zibozdi, S. Ghan, M. Chin, P. Ginoux, T. Takemura, I. Tegen, D. Koch, R. Kahn, E. Vermote, L. Stowe, O. Torres, M. Mishchenko, and I. Geogdzhayev, 2001: How well do aerosol retrievals from satellites and representation in global circulation models match ground-based AERONET aerosol statistics? In *Remote Sensing and Climate Modeling: Synergies and Limitations*. Kluwer Academic Publishers, in press.
- Krotkov, N. A., O. Torres, C. Seftor, A. J. Krueger, A. Kostinski, W. I. Rose, G. J. S. Bluth, D. Schneider, and S. J. Schaefer, 1999: Comparison of TOMS and AVHRR volcanic ash retrievals from the August 1992 eruption of Mt. Spurr. *Geophys. Res. Lett.*, **26**, 455–458.
- Lacis, A. A., B. E. Carlson, and J. E. Hansen, (2000): Retrieval of atmospheric NO<sub>2</sub>, O<sub>3</sub>, aerosol optical depth, effective radius and variance information from SAGE II multi-spectral

- extinction measurements. *Appl. Math. Comput.*, **116**, 133–151.
- Lacis, A. A. and V. Oinas, 1991: A description of the correlated k-distribution method for modeling non-grey gaseous absorption, thermal emission, and multiple scattering in vertically inhomogeneous atmospheres. *J. Geophys. Res.* **96**, 9027–9063.
- Liou, K. N., and Y. Takano, 1994: Light scattering by nonspherical particles: Remote sensing and climatic applications. *Atmos. Res.*, **31**, 271–298.
- Masuda, K., T. Takashima, Y. Kawata, A. Yamazaki, and M. Sasaki, 2000: Retrieval of aerosol optical properties over the ocean using multispectral polarization measurements from space. *Appl. Math. Comput.*, **116**, 103–114.
- McClatchey, R. A., R. W. Fenn, J. E. A. Selby, F. E. Volz, and J. S. Garing, 1972: *Optical properties of the atmosphere, Environ. Res. Paper 411*, Air Force Cambridge Research Laboratory, Bedford, Mass.
- Mishchenko, M. I., and L. D. Travis, 1997: Satellite retrieval of aerosol properties over the ocean using polarization as well as intensity of reflected sunlight. *J. Geophys. Res.*, **102**, 16,989–17,013.
- Mishchenko, M. I., A. A. Lacis, B. E. Carlson, and L. D. Travis, 1995: Nonsphericity of dust-like tropospheric aerosols: Implications for aerosol remote sensing and climate modeling. *Geophys. Res. Lett.*, **22**, 1077–1080.
- Mishchenko, M. I., L. D. Travis, W. B. Rossow, B. Cairns, and B. E. Carlson, 1997a: Retrieving CCN column density from single channel measurements of reflected sunlight over the ocean: A sensitivity study. *Geophys. Res. Lett.*, **24**, 2655–2658.
- Mishchenko, M. I., Travis, L. D., Kahn, R. A., and West, R. A., 1997b: Modeling phase functions for dustlike tropospheric aerosols using a shape mixture of randomly oriented polydisperse spheroids. *J. Geophys. Res.*, **102**, 16,831–16,847.
- Mishchenko, M. I., I. V. Geogdzhayev, B. Cairns, W. B. Rossow, and A. A. Lacis, 1999a: Aerosol retrievals over ocean using channel 1 and 2 AVHRR data: A sensitivity analysis. *Appl. Opt.*, **38**, 7325–7341.

- Mishchenko, M. I., J. M. Dlugach, E. G. Yanovitskij, and N. T. Zakharova, 1999b: Bidirectional reflectance of flat, optically thick particulate layers: An efficient radiative transfer solution and applications to snow and soil surfaces. *J. Quant. Spectrosc. Radiat. Transfer*, **63**, 409–432.
- Mishchenko, M. I., L. D. Travis, and A. A. Lacis, 2002. *Scattering, Absorption, and Emission of Light by Small Particles*. Cambridge University Press.
- Moore, K. D., K. J. Voss, and H. R. Gordon, 1998: Spectral reflectance of whitecaps: Instrumentation, calibration, and performance in coastal waters. *J. Atmos. Oceanic Technol.*, **15**, 496–509.
- Mukai, S., and I. Sano, 1999: Retrieval algorithm for atmospheric aerosols based on multi-angle viewing of ADEOS/POLDER. *Earth Planets Space*, **51**, 1247–1254.
- Nakajima, T., and A. Higurashi, 1998: A use of two-channel radiances for an aerosol characterization from space. *Geophys. Res. Lett.*, **25**, 3815–3818.
- Penner, J. E., S. Y. Zhang, M. Chin, C. C. Chuang, J. Feichter, Y. Feng, P. Ginoux, M. Herzog, A. Higurashi, D. Koch, C. Land, U. Lohmann, M. Mishchenko, T. Nakajima, G. Pitari, B. Soden, I. Tegen, L. Stowe, and I. Geogdzhayev, 2001: A comparison of model- and satellite-derived optical depth and reflectivity. *J. Atmos. Sci.*, this issue.
- Raes, F., T. Bates, F. McGovern, and M. van Liedekerke, 2000: The 2nd Aerosol Characterization Experiment (ACE-2): General overview and main results. *Tellus B*, **52**, 111–125.
- Rao, C. R. N., and J. Chen, 1995: Inter-satellite calibration linkages for the visible and near infrared channels of the AVHRR on the NOAA-7,9 and 11 spacecraft. *Int. J. Remote Sens.*, **16**, 1931-1942
- Rao, C. R. N., J. Chen, F. W. Staylor, P. Abel, Y. J. Kaufman, E. Vermote, and W. B. Rossow, 1993: Degradation of the visible and near-infrared channels of the Advanced Very High Resolution Radiometer on NOAA-9 spacecraft: Assessment and recommendations for corrections. *NOAA Technical Report NESDIS 70*, 25 pp.
- Rossow, W. B., and L. C. Garder, 1993: Cloud detection using satellite measurements of infrared

- and visible radiances for ISCCP. *J. Clim.*, **6**, 2341–2369.
- Rossow, W. B., and R. A. Schiffer, 1999: Advances in understanding clouds from ISCCP. *Bull. Am. Meteorol. Soc.*, **80**, 2261–2287.
- Rossow, W. B., A. W. Walker, D. E. Beuschel, and M. D. Roiter, 1996: *International Satellite Cloud Climatology Project (ISCCP) Documentation of New Cloud Data Sets*. World Climate Research Programme, WMO/TD-No. 737, 115 pp.
- Russell, P. B., and J. Heintzenberg, 2000: An overview of the ACE-2 clear sky column closure experiment (CLEARCOLUMN). *Tellus B*, **52**, 463–483.
- Russell, P. B., J. M. Livingston, P. Hignett, S. Kinne, J. Wong, A. Chien, R. Bergstrom, P. Durkee, and P. V. Hobbs, 1999: Aerosol-induced radiative flux changes off the United States mid-Atlantic coast: Comparison of values calculated from sunphotometer and in situ data with those measured by airborne pyranometer. *J. Geophys. Res.*, **104**, 2289–2307.
- Schwartz, S. E., and A. Slingo, 1996: Enhanced shortwave cloud radiative forcing due to anthropogenic aerosols. In *Clouds, Chemistry, and Climate*, edited by P. J. Crutzen and V. Ramanathan, Springer-Verlag, pp. 191–236.
- Spinrad, R. W., K. L. Carder, M. J. Perry, 1994: *Ocean Optics*. Oxford University Press, 283 pp.
- Stowe, L. L., A. M. Ignatov, and R. R. Singh, 1997: Development, validation, and potential enhancements to the second-generation operational aerosol product at the National Environmental Satellite, Data, and Information Service of the National Oceanic and Atmospheric Administration. *J. Geophys. Res.*, **102**, 16,923–16,934.
- Stowe, L. L., P. A. Davis, E. P. McClain, 1999: Scientific basis and initial evaluation of the CLAVR-1 global clear/cloud classification algorithm for the Advanced Very High Resolution Radiometer. *J. Atmos. Oceanic Technol.*, **16**, 656–681
- Tanré, D., Y. J. Kaufman, M. Herman, and S. Mattoo, 1997: Remote sensing of aerosol properties over oceans using the MODIS/EOS spectral radiances. *J. Geophys. Res.*, **102**, 16,971–16,988.
- Tsang, L., J. A. Kong, and R. T. Shin, 1985: *Theory of Microwave Remote Sensing*. John Wiley and Sons, 613 pp.

- Wagner R., S. Nemesure, and S. E. Schwartz, 1997 : Aerosol optical depth over oceans: High space- and time-resolution retrieval and error budget from satellite radiometry. *J. Atmos. Oceanic Technol.*, **14**, 577–590.
- Yang, P., K. N. Liou, M. I. Mishchenko, and B.-C. Gao, 2000: Efficient finite-difference time-domain scheme for light scattering by dielectric particles: Application to aerosols. *Appl. Opt.*, **39**, 3727–3737.
- Zhao, T. X.-P., L. L. Stowe, A. Ignatov, A. Smirnov, D. Crosby, J. Sapper, and C. R. McClain, 2001: Development of a global validation package for satellite oceanic aerosol optical thickness retrieval based on AERONET observations and its application to NOAA/NESDIS operational aerosol retrievals. *J. Atmos. Sci.*, this issue.

## Figure captions

Fig. 1. Ratio of the phase function calculated for the power law size distribution of spherical aerosols assuming the refractive index  $m = 1.5+0.003i$  to that calculated with  $m = 1.5+0.005i$  versus scattering angle and Ångström exponent.

Fig. 2. Single-scattering albedo versus Ångström exponent for two values of the refractive index. The dot-dashed curve shows the ratio of the two single-scattering albedos.

Fig. 3. Monthly mean aerosol optical thickness and Ångström exponent for July 1988. (a) and (b): The average  $\tau$  and  $A$  values are computed using all cloud-free pixels. (c) and (d): The average  $\tau$  and  $A$  values are computed using only pixels with  $0 < A < 1.75$ .

Fig. 4. Frequency of occurrence of Ångström exponent values for the period Feb 1985–Nov 1988 (NOAA-9 dataset).

Fig. 5. (a): Ratio of monthly mean aerosol optical thicknesses for July 1986 retrieved with modified (reduced by one count) and original channel 2 radiances. (b): As in (a), but for the Ångström exponent difference. (c) and (d): As in (a) and (b), respectively, but with channel 2 radiances increased by one count.

Fig. 6. (a): Ratio of monthly mean aerosol optical thicknesses retrieved with the bimodal size distribution of Eq. (6) and the power law distribution of Eq. (1). (b): As in (a), but for the difference of constrained monthly mean Ångström exponents. (c): As in (a), but for the CCN column number density retrieved with constrained Ångström exponents. (d): As in (a), but for the CCN column number density retrieved with unconstrained Ångström exponents.

Fig. 7. Extinction cross section per particle versus Ångström exponent for the bimodal size distribution of Eq. (6) and the power law distribution of Eq. (1) and the ratio of the former to the latter.

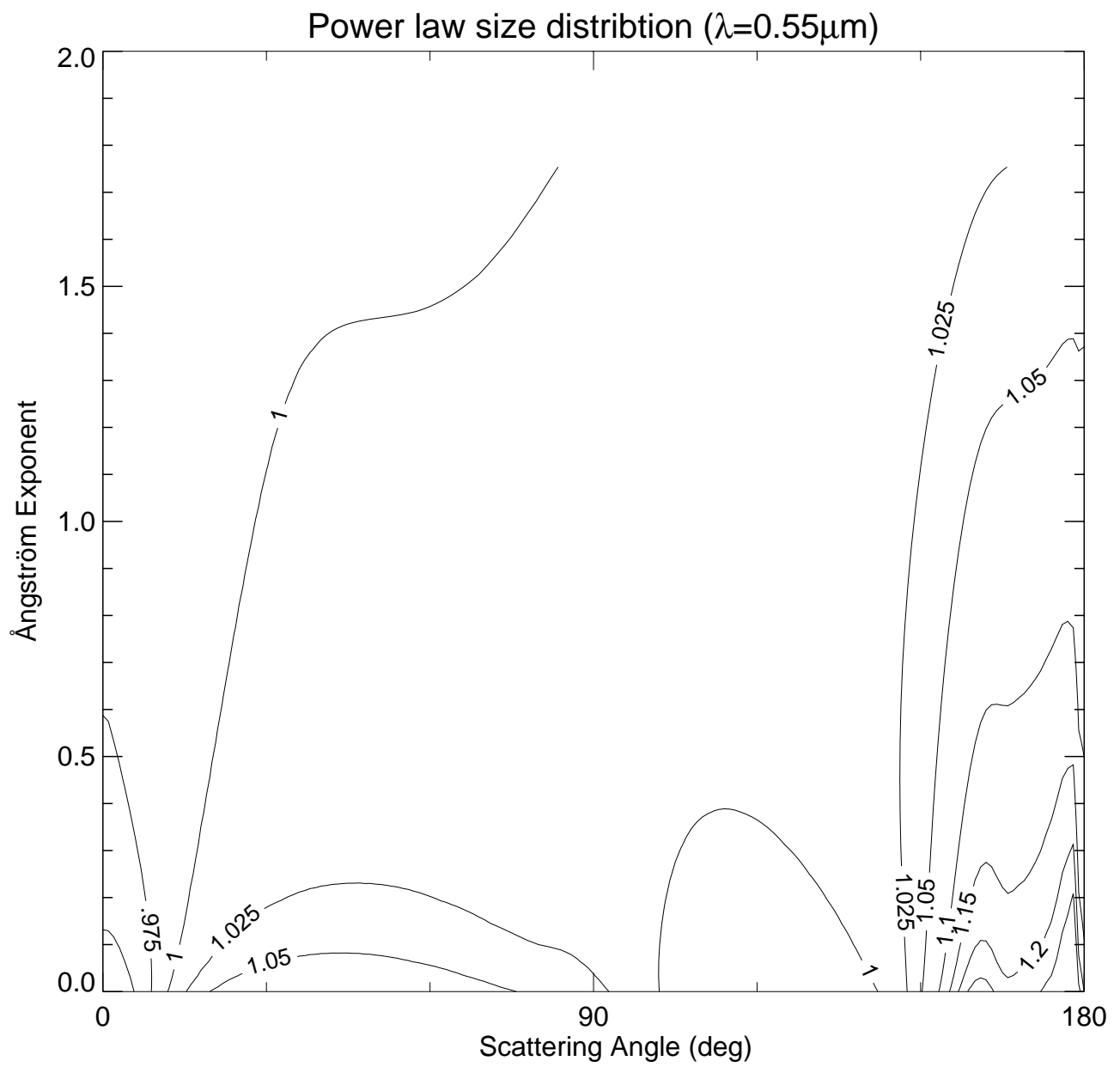
Fig. 8. (a) Ratio of monthly mean aerosol optical thicknesses retrieved assuming SSM/I-derived wind speed values and a fixed wind speed value of 7 m/s for July 1988. (b) As in (a), but for the difference of constrained Ångström exponents.

Fig. 9. Global and hemispherical monthly averages of the aerosol optical thickness and

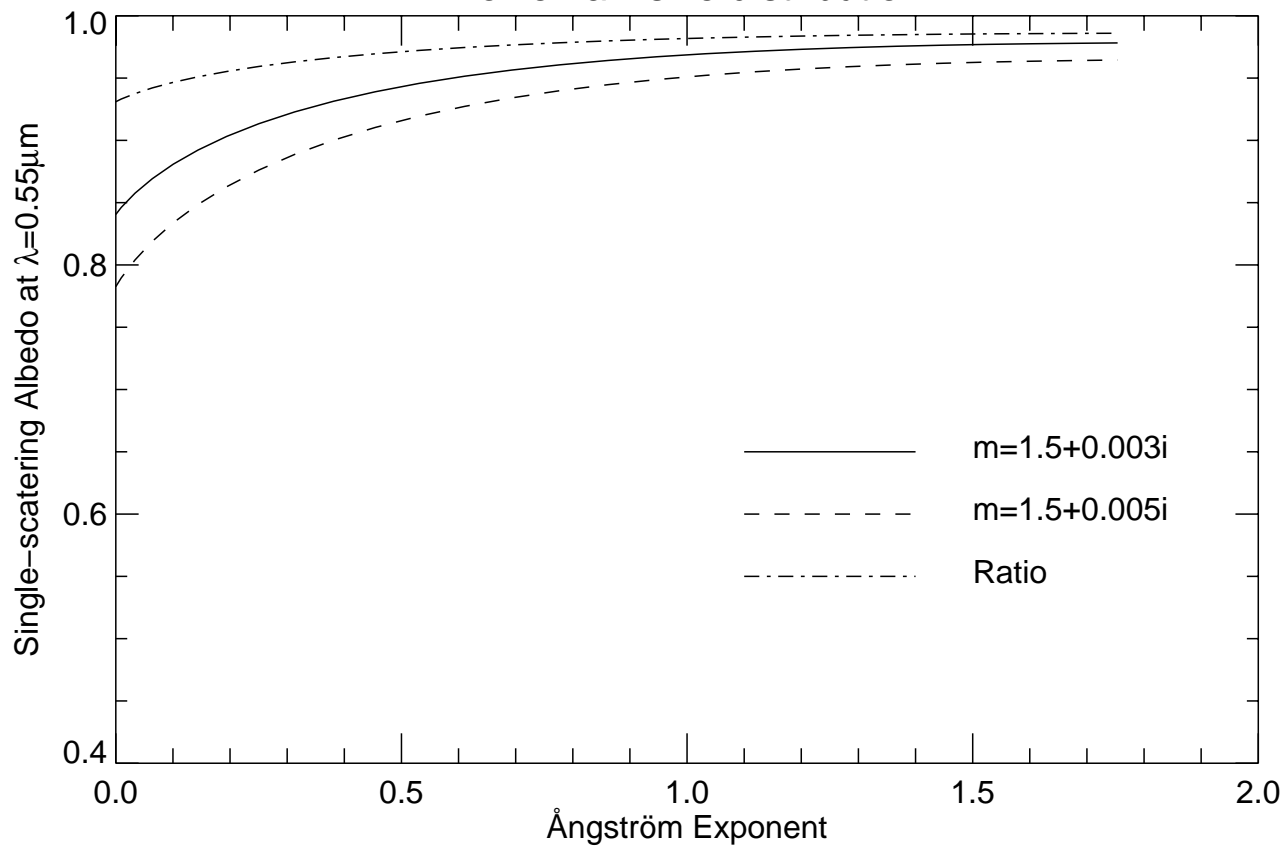
constrained Ångström exponent for the period of July 1983–August 1994.

Fig. 10. Global and hemispherical monthly averages of the unconstrained Ångström exponent for the period of Jul 1983–Aug 1994.

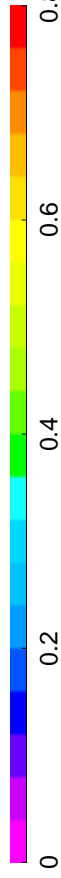
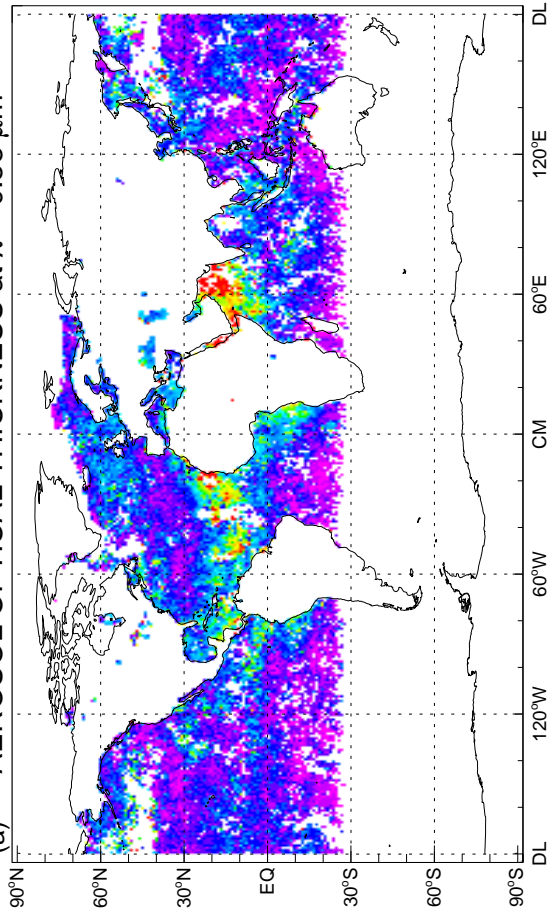
Fig. 11. Monthly mean zonal values of the aerosol optical thickness derived from the NOAA-9 dataset.



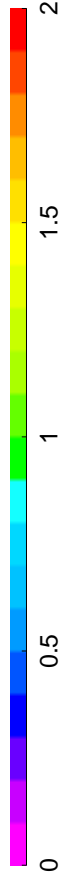
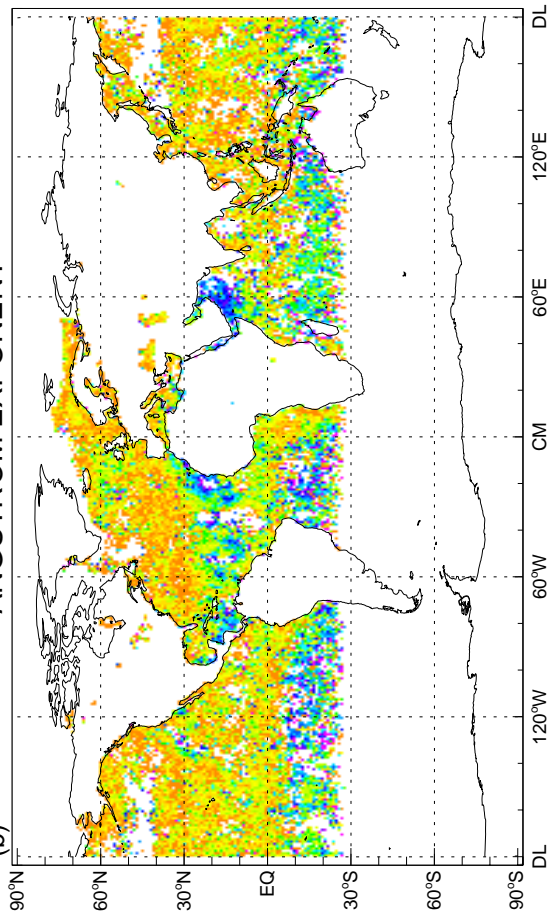
Power law size distribution



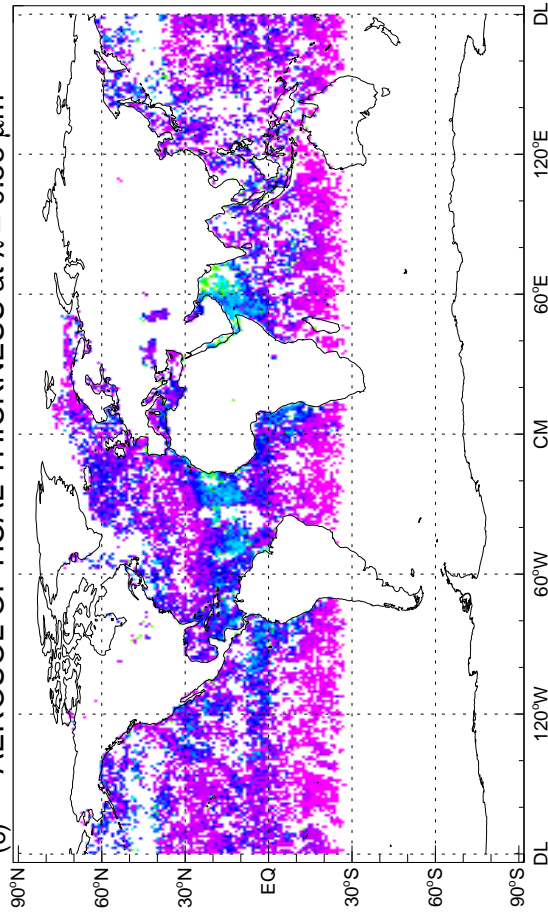
(a) AEROSOL OPTICAL THICKNESS at  $\lambda = 0.55 \mu\text{m}$



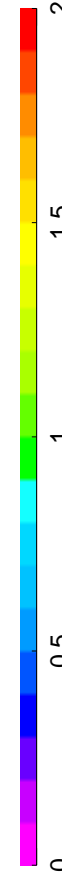
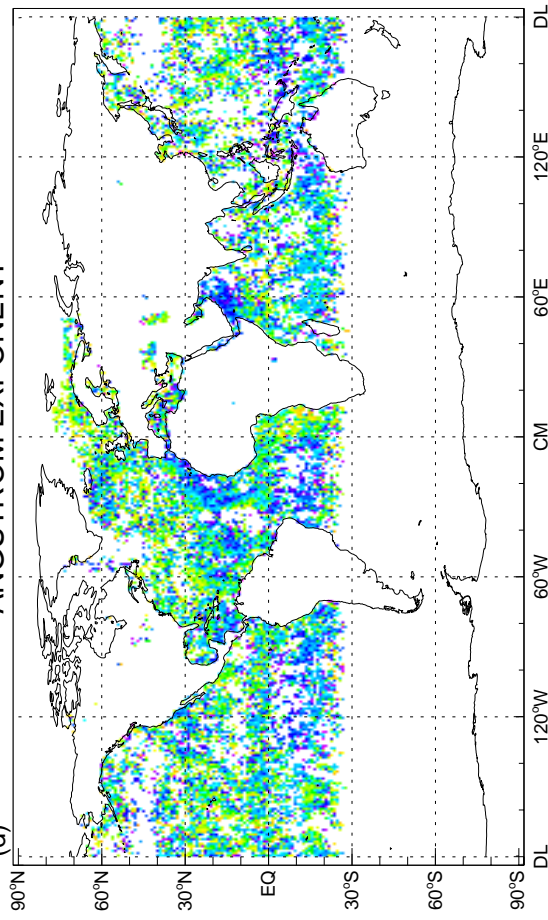
(b) ÅNGSTRÖM EXPONENT

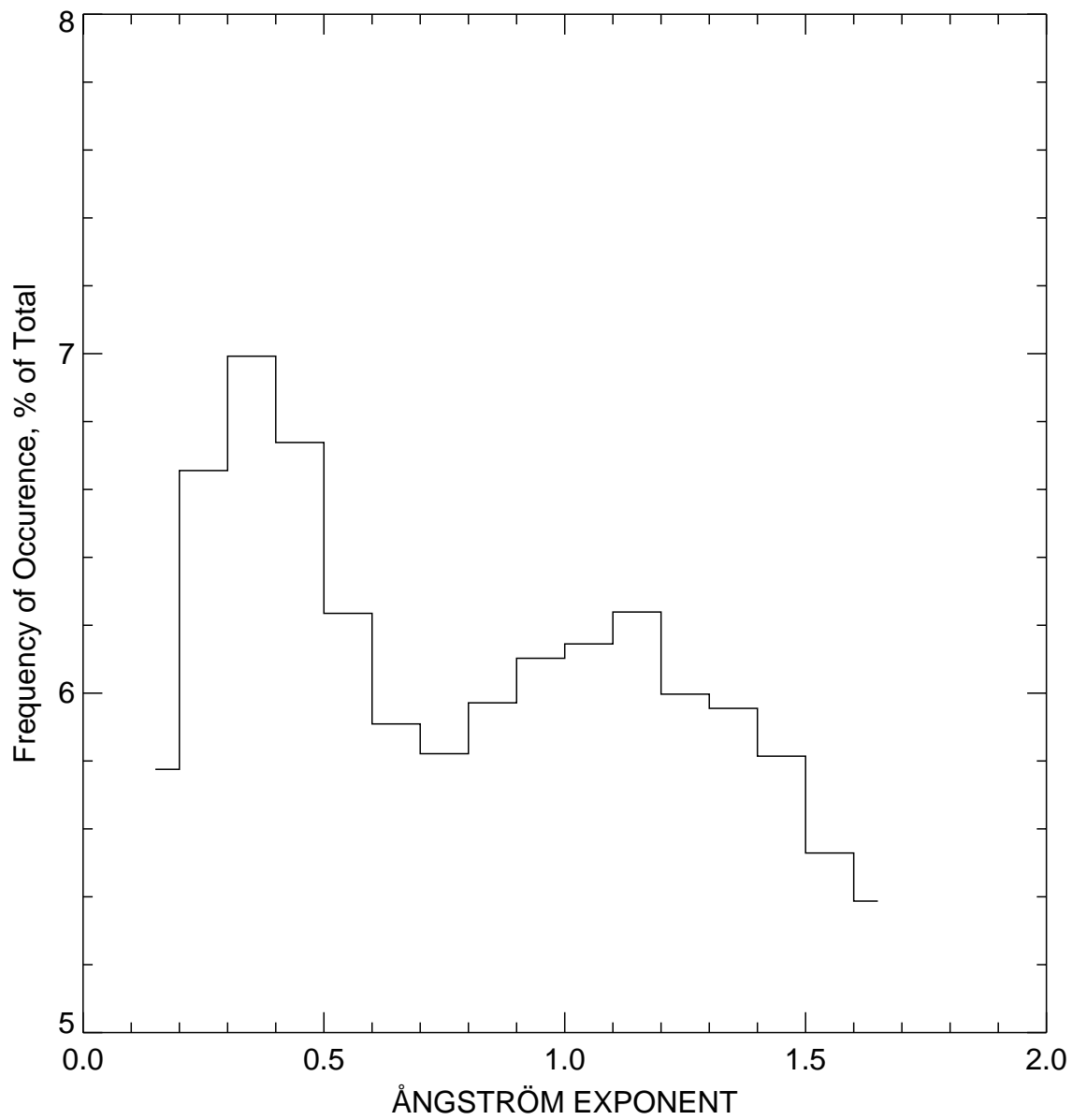


(c) AEROSOL OPTICAL THICKNESS at  $\lambda = 0.55 \mu\text{m}$

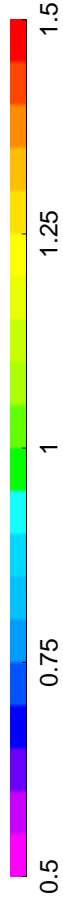
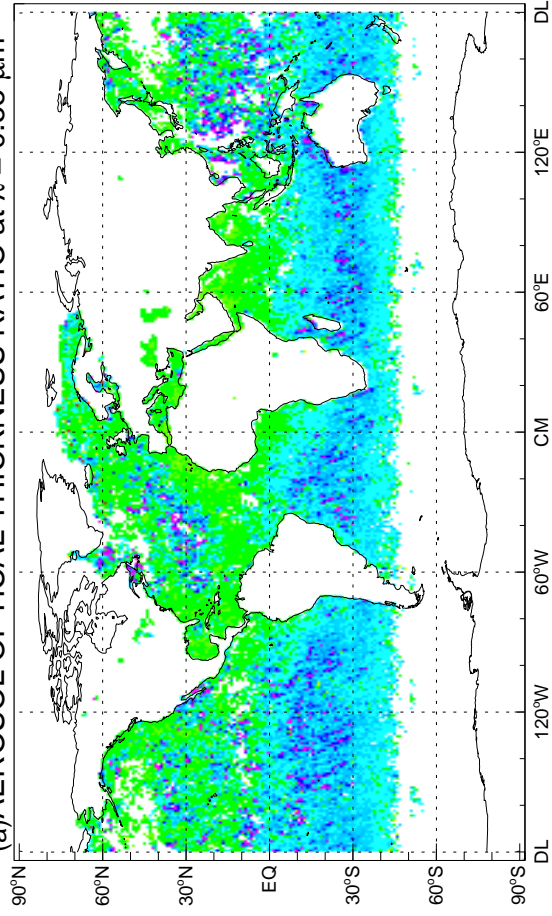


(d) ÅNGSTRÖM EXPONENT

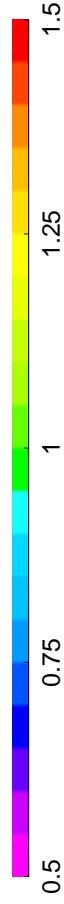
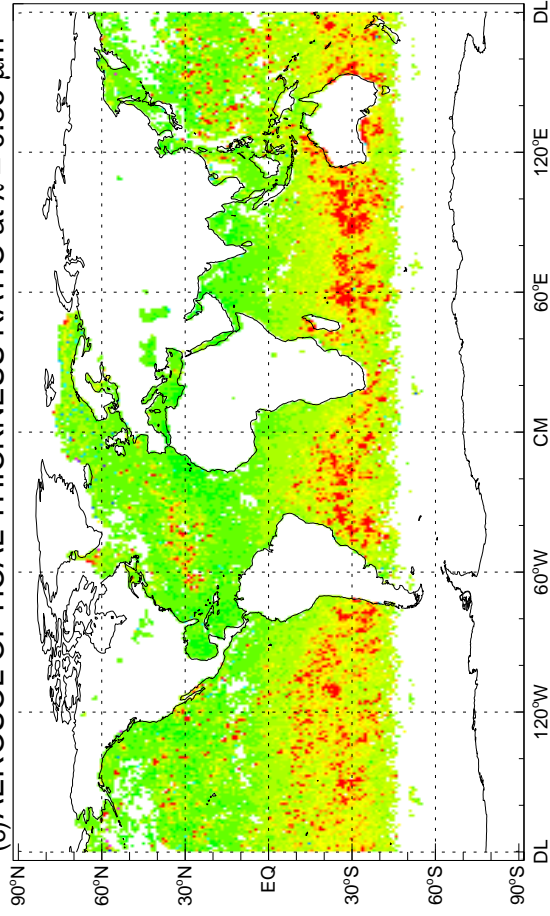




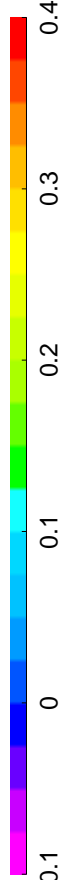
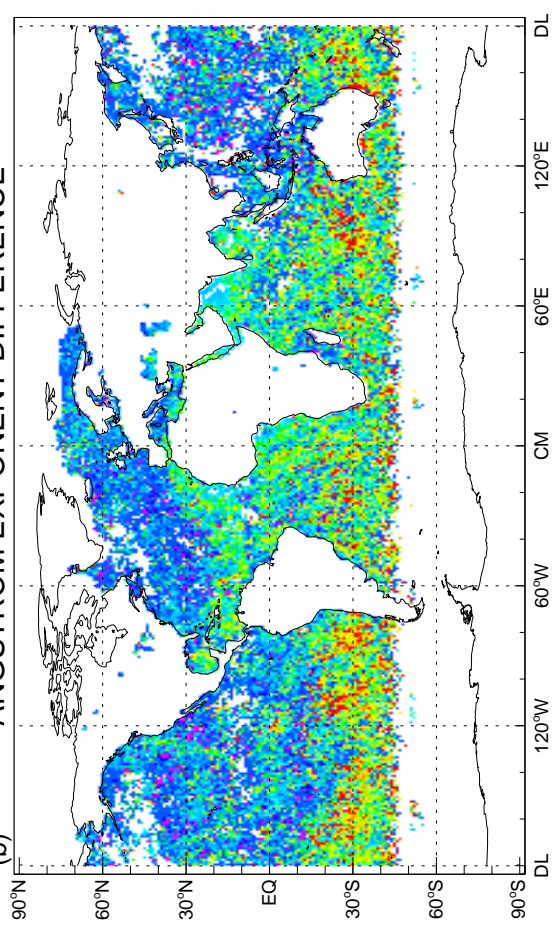
(a) AEROSOL OPTICAL THICKNESS RATIO at  $\lambda = 0.55 \mu\text{m}$



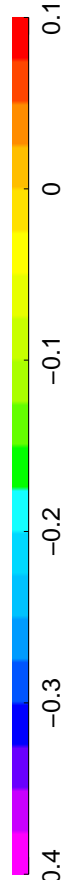
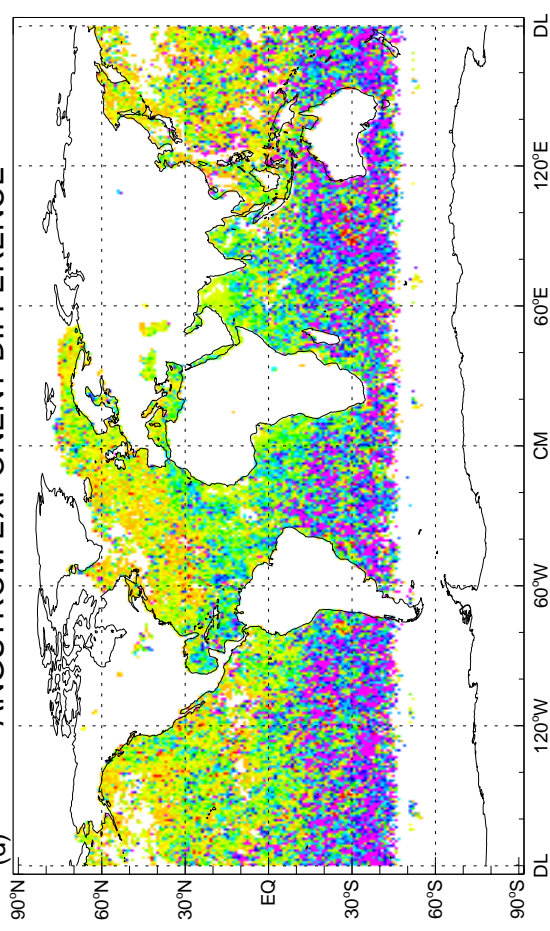
(c) AEROSOL OPTICAL THICKNESS RATIO at  $\lambda = 0.55 \mu\text{m}$



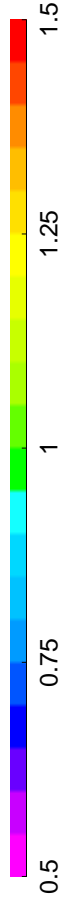
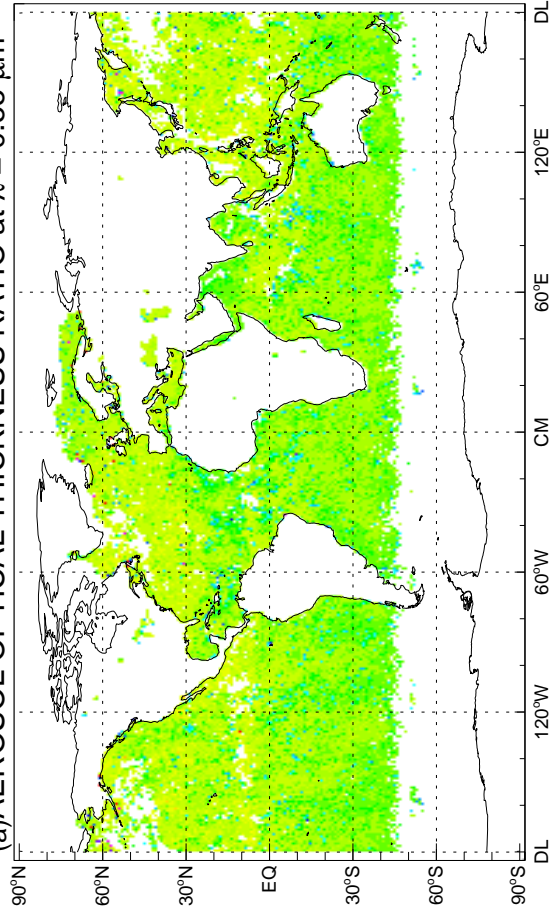
(b) ÅNGSTRÖM EXPONENT DIFFERENCE



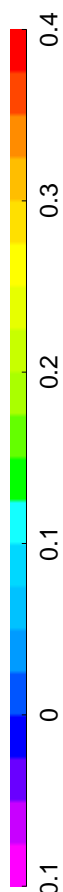
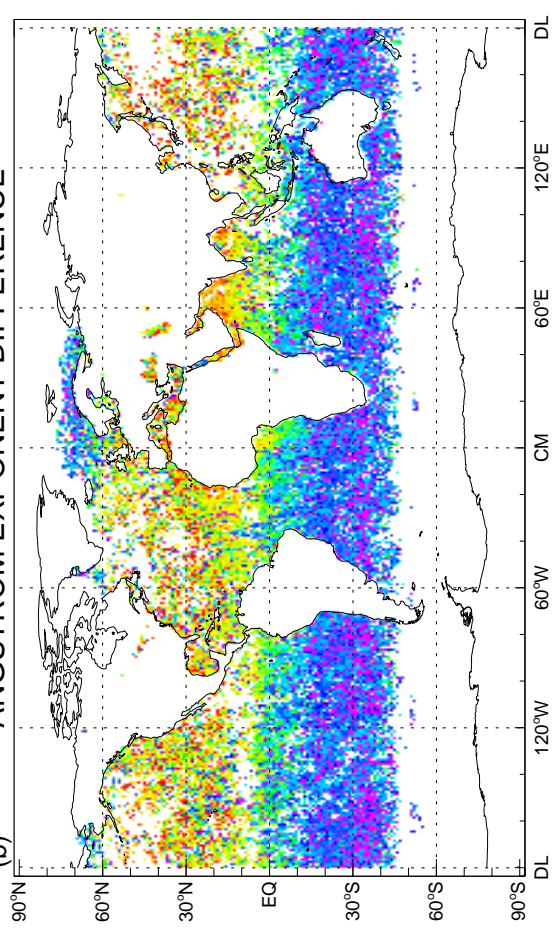
(d) ÅNGSTRÖM EXPONENT DIFFERENCE



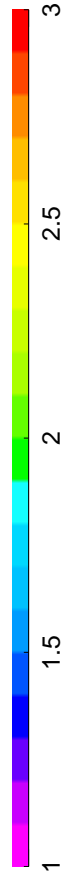
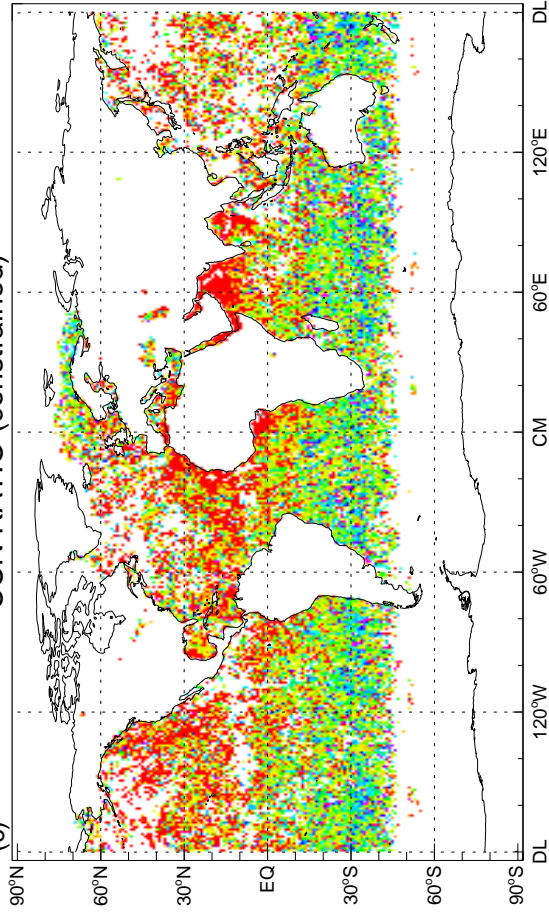
(a) AEROSOL OPTICAL THICKNESS RATIO at  $\lambda = 0.55 \mu\text{m}$



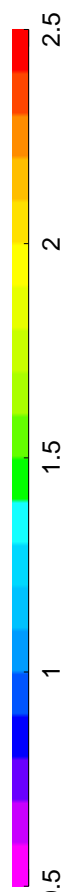
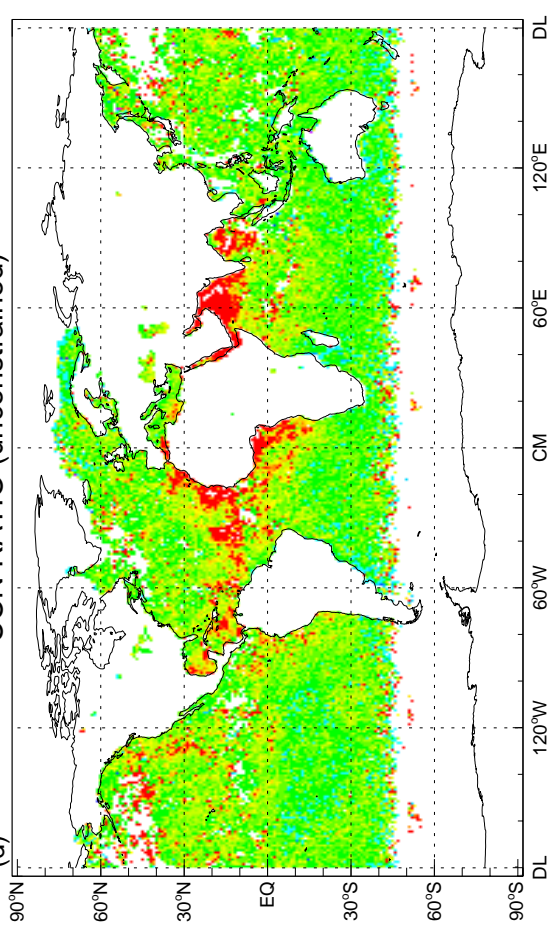
(b) ÅNGSTRÖM EXPONENT DIFFERENCE

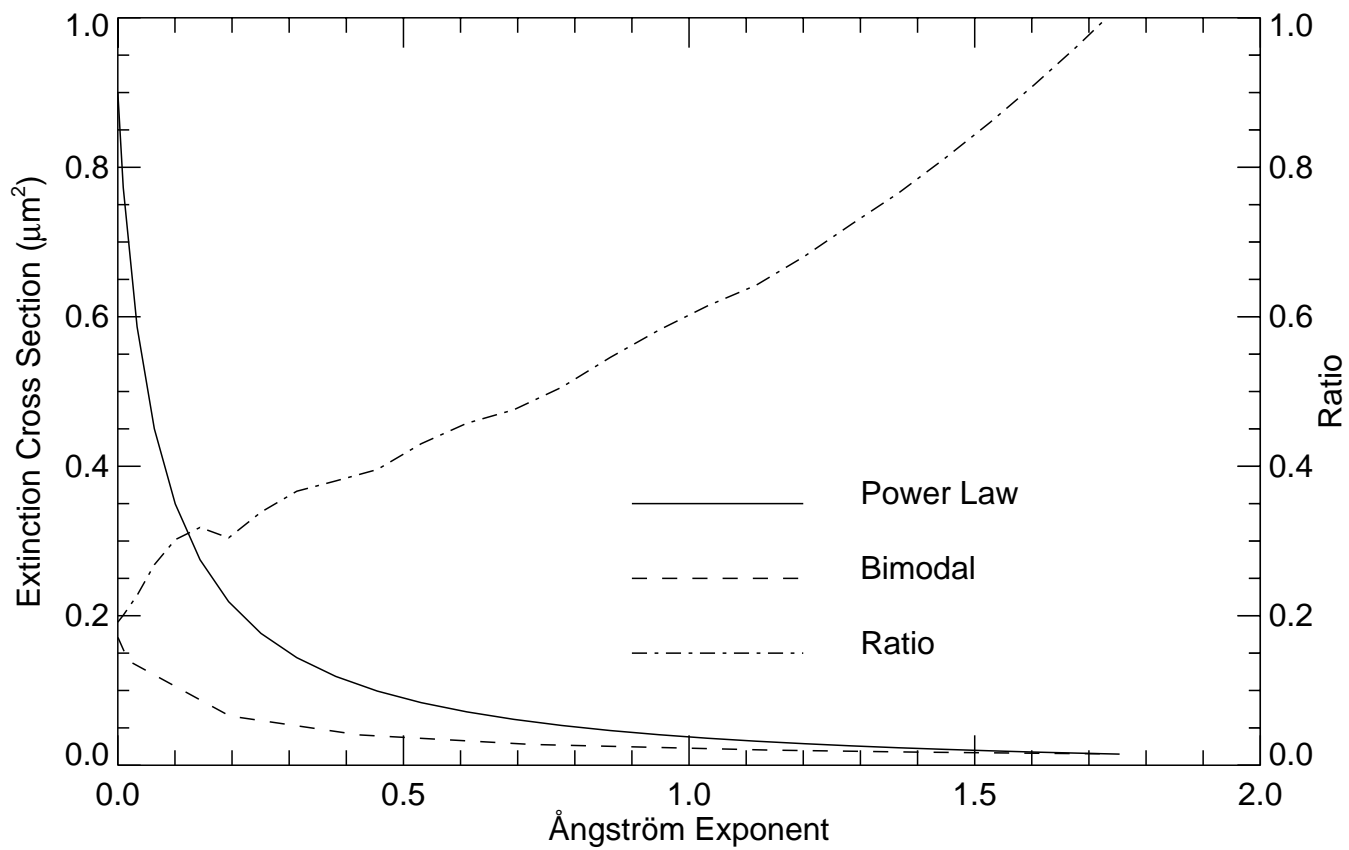


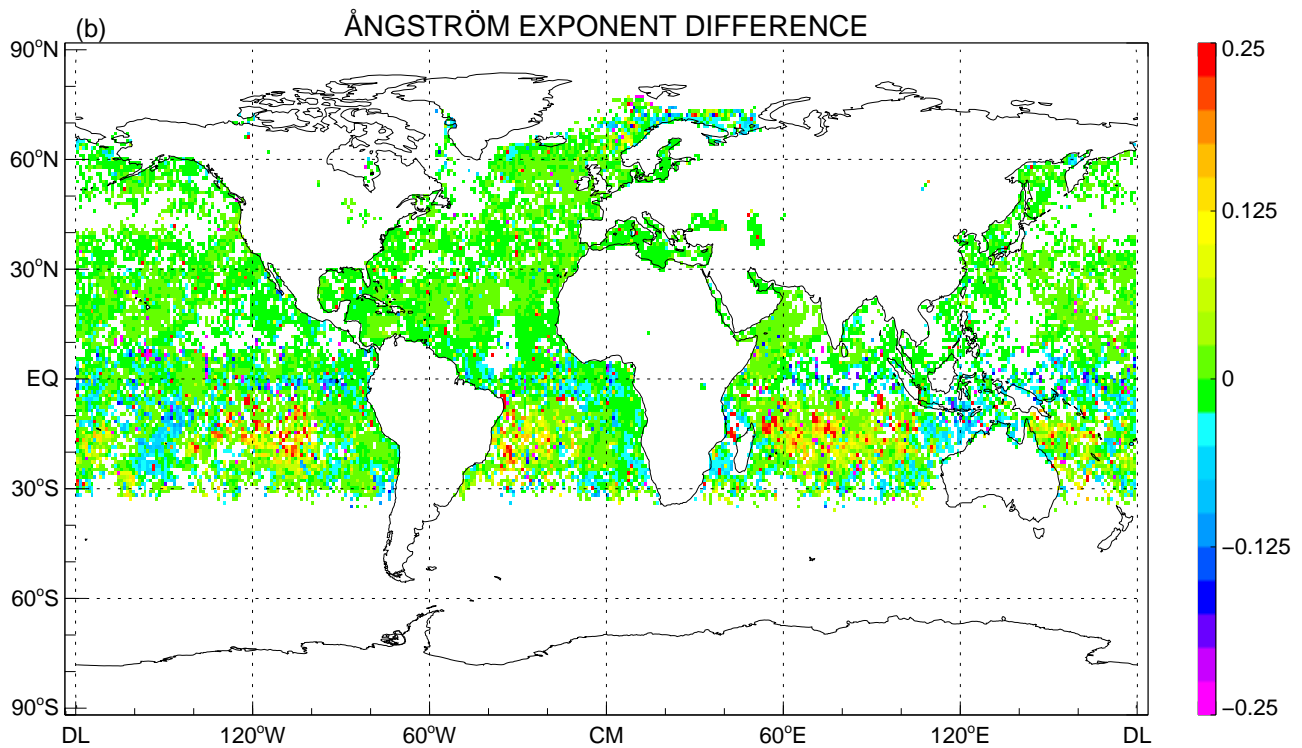
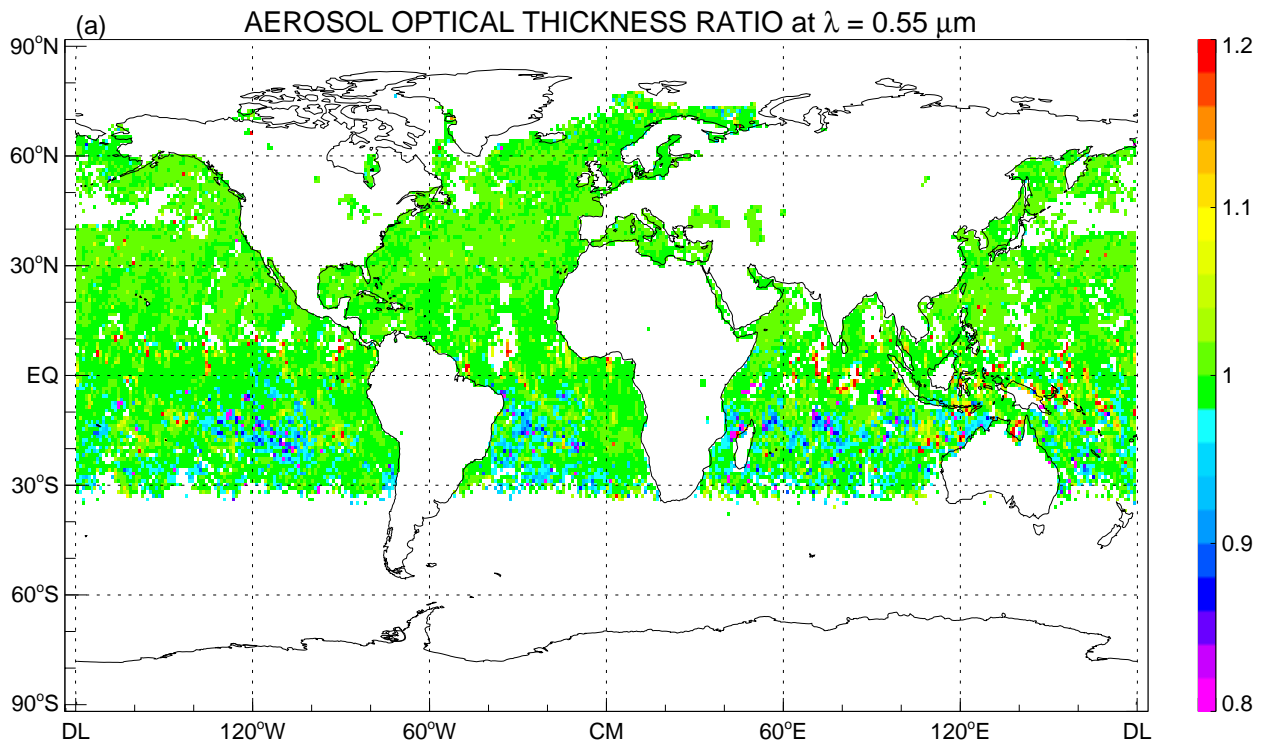
(c) CCN RATIO (constrained)

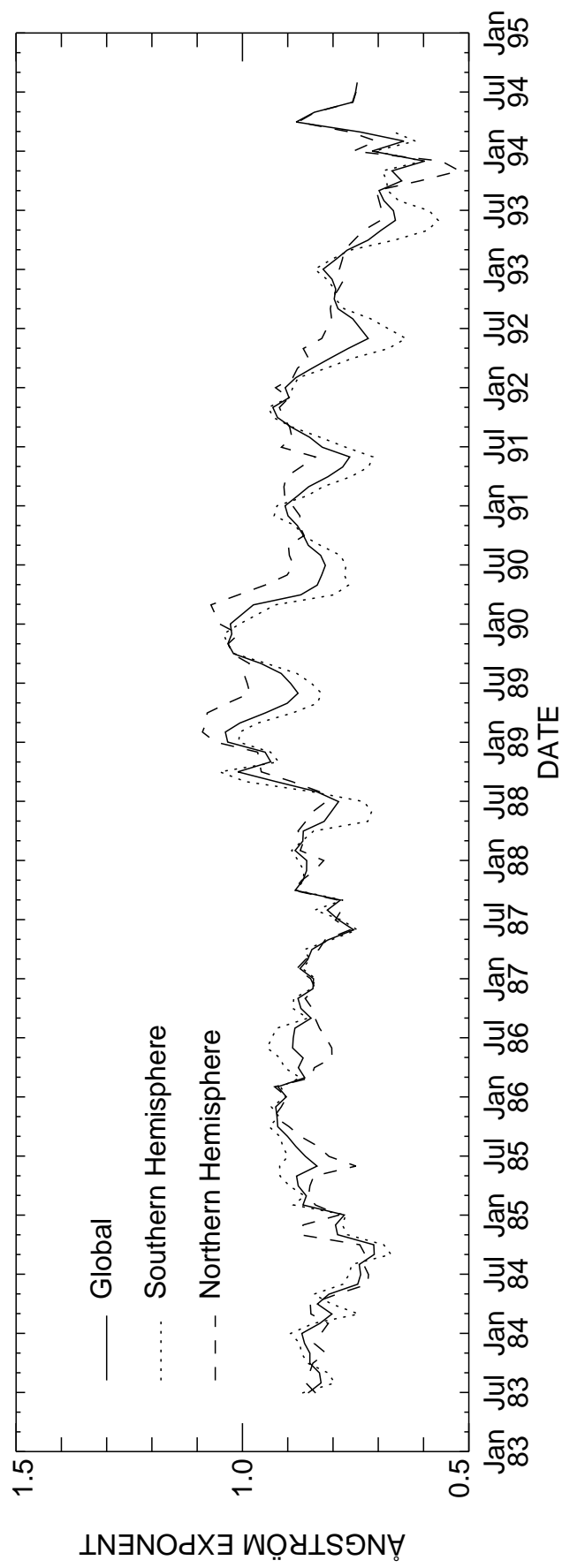
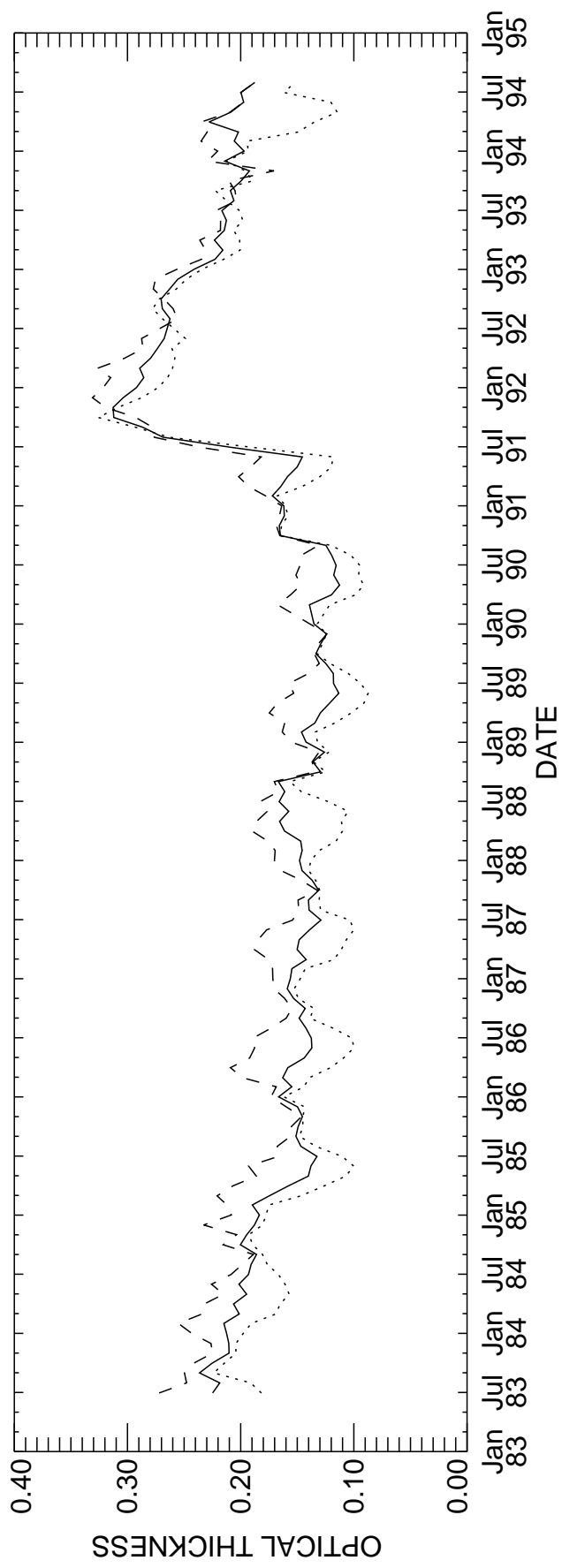


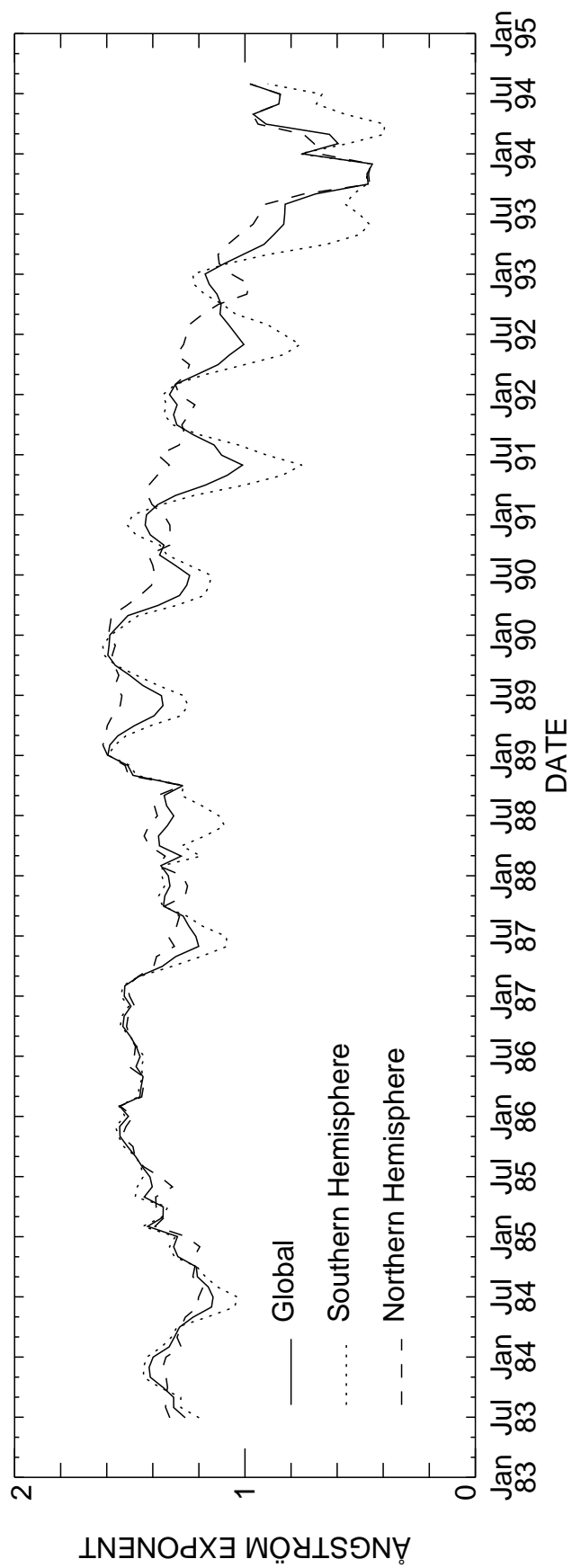
(d) CCN RATIO (unconstrained)











# AEROSOL OPTICAL THICKNESS at $\lambda = 0.55 \mu\text{m}$

